J. Ocean Univ. China (Oceanic and Coastal Sea Research)
https://doi.org/10.1007/s11802-022-4881-x
ISSN 1672-5182, 2022 21 (4): 998-1016
http://www.ouc.edu.cn/xbywb/
E-mail:xbywb@ouc.edu.cn

Expression Characteristics and Putative Functions of KIF3A/KIF3B During Spermiogenesis of *Phascolosoma esculenta*

DU Chen[1)], MU Danli [1)], GAO Xinming[1)], LUO Shengyu[1)], WANG Jianping[2)], JIN Shan[1)], and ZHU Junquan[1), *]

1) *Key Laboratory of Applied Marine Biotechnology by the Ministry of Education*, *Ningbo University*, *Ningbo* 315211, *China*
2) *Ningbo Academy of Oceanology and Fisheries*, *Ningbo* 315012, *China*

(Received December 15, 2020; revised March 22, 2021; accepted July 6, 2021)

Abstract The microtubule (MT)-associated proteins KIF3A and KIF3B are ubiquitously expressed in a wide range of taxa. This study investigated the functions of these proteins in spermiogenesis, which involves various MT-dependent processes, in *Phascolosoma esculenta*. We cloned the complete cDNA of *Pe*-KIF3A/3B. Structural predictions showed that *Pe*-KIF3A/3B are composed of a highly conserved motor domain, a coiled-coil domain, and a tail domain. Real-time quantitative PCR showed that *Pe-kif3a/3b* are expressed in all tissues evaluated, with the highest levels in sperm masses. Fluorescence *in situ* hybridization and immunofluorescence were employed to analyze the dynamic expression patterns of KIF3A/3B during spermiogenesis. *Pe*-KIF3A/3B consistently co-localized with MTs at all stages of spermiogenesis, indicating their potential functions in cargo trafficking. *Pe*-KIF3A/3B co-localized with mitochondria, suggesting that they may mediate mitochondrial movement. In late-stage spermatids and mature sperm, co-localization was detected in the midpiece, suggesting that *Pe*-KIF3A/3B could facilitate midpiece formation. The co-localization of *Pe*-KIF3A and *Pe*-KIF3B at all stages of spermiogenesis suggests their function as the heterodimeric KIF3AB. Basing on the observed temporal and spatial expression patterns of *Pe*-KIF3A/3B, MTs, and mitochondria in our study, we suggest that heterodimer KIF3AB has a potential role in acrosome biogenesis, sperm head remodeling, enflagellation, and mitochondrial migration during spermiogenesis in *P. esculenta.* In addition, our study on the morphological characteristics of spermatogenic cells provided fundamental data on the reproductive biology of *P. esculenta.*

Key words *Phascolosoma esculenta*; spermiogenesis; kinesin 3A/3B; heterodimerization

1 Introduction

In general, spermatogenesis can be divided into three phases: a mitotic phase in which spermatogonia produce spermatocytes, a meiotic phase in which spermatocytes produce haploid round spermatids, and a haploid phase (Rupik *et al*., 2011; O'Donnell and O'Bryan, 2014). During these phases, biochemical and morphological changes in germ cells vary considerably among species, especially among invertebrates. Invertebrate sperms can be divided into several groups according to their differences in the head, flagellum, and acrosome. For example, most invertebrate sperms, such as the sperms of mollusks *Octopus tankankeei* (Dang *et al*., 2012) and *Saccostrea forskali* (Nuurai *et al*., 2016), contain an acrosome and a long flagellum. However, the amoeboid-shaped sperms of the nematode *Caenorhabditis elegans* lack the acrosome and flagellum (Singson 2001). The none-flagellate sperms of the crustaceans *Palaemon carinicauda* and *Eriocheir sinensis* have spiked heads (Lu *et al*., 2014; Zhao *et al*., 2017). For flagellate sperms, the integrity of the sperm tail is essential for sperm motility and fertilization (Lehti and Sironen, 2016). The midpiece is a conserved structure of sperm tails. It consists of the intermediate axoneme and peripheral mitochondria, which provide energy for sperm motility (Ramalhosantos *et al*., 2009; Amaral *et al*., 2013). The acrosome is a landmark for spermatid polarity, and it is formed by secretory vesicles from the Golgi apparatus. The acrosome has important functions in fertilization (Yang and Sperry, 2003). The acrosome biogenesis, head deformation, and tail formation of sperm are clearly microtubule (MT)-dependent processes (Moreno *et al*., 2006; O'Donnell and O'Bryan, 2014).

MTs serve as the rails for intracellular transport, enabling motor proteins to 'walk along'. Enflagellation and spermatid nuclear reshaping rely on MTs and MT-associated motor proteins (Fawcett *et al*., 1971; O'Donnell and O'Bryan, 2014; Zhao *et al*., 2017). The Kinesin superfamily is a group of MT-dependent proteins involved in intracellular transport (Hirokawa and Noda, 2008). Among KIFs, Kinesin II controls anterograde trafficking (Funa-

* Corresponding author. E-mail: zhujunquan@nbu.edu.cn

bashi *et al*., 2018). In mammals, Kinesin II genes include *KIF3A*, *KIF3B*, *KIF3C*, and *KIF17* (Gilbert *et al*., 2018). This subfamily is ubiquitously expressed at high levels in organisms (Henson *et al*., 1997; Marszalek and Goldstein, 2000). As members of Kinesin II, KIF3A and KIF3B are expressed in various tissues and are highly expressed in the testis and nervous system (Hall *et al*., 1992; Henson *et al*., 1997; Dang *et al*., 2012; Lehti *et al*., 2013). KIF3C and KIF17 are only highly expressed in the nervous system (Yang *et al*., 2001). KIF3A/3B serve important functions in the anterograde transport of membrane-bound organelles (Marszalek and Goldstein, 2000; Zhao *et al*., 2017) and newly synthesized proteins from the endoplasmic reticulum (Stauber *et al*., 2006). KIF3A/3B are also involved in intraflagellar transport (IFT). They can transport large protein complexes from the base to the tip of the cilia and flagella (Pan *et al*., 2006; Scholey, 2012). They also participate in cell division (Fan and Beck, 2004; Haraguchi *et al*., 2006; Kodani *et al*., 2013; Shen *et al*., 2017). The functions of KIF3A and KIF3B in spermiogenesis have become a major focus of research. In the reptile *Cynops orientalis*, *kif3a* is highly expressed in the testis and spermatids (Hu *et al*., 2012). In the cephalopod *Octopus tankahkeei*, KIF3A/3B play potential roles in nuclear deformation and enflagellation (Wang *et al*., 2010; Dang *et al*., 2012). In the crustaceans *Palaemon carinicauda* and *E. sinensis*, KIF3A/3B are involved in acrosome formation and nuclear reshaping (Lu *et al*., 2014; Zhao *et al*., 2017). In sand dollar sperm, KIF3A/3B are located in the midpiece and flagellum (Henson *et al*., 1997). In *Boleophthalmus pectinirostris*, KIF3A/3B may transport mitochondria during midpiece formation (Zhao *et al*., 2018). In murine testes, KIF3A/3B are involved in sperm tail formation and head shaping (Miller *et al*., 1999b; Lehti *et al*., 2013). In brief, KIF3A/3B are essential for spermiogenesis in various animals, especially in the sperm head deformation and tail formation. However, the functions of KIF3A/3B in Sipuncula have not been determined. Moreover, species belonging to Sipuncula developed specialized reproductive strategies. During spermatogenesis, the ribbonlike testis releases spermatocytes into the coelomic fluid, where germ cells gather into cell masses and grow into mature spermatozoa. After storage in the nephridia for a brief period, fertilization in sipunculids is completed *in vitro* (Staton, 1994). The unique aspects of this process emphasize the importance of Sipuncula research, particularly the studies of spermiogenesis. *Phascolosoma esculenta* is an economically valuable endemic Chinese species belonging to Sipuncula (Li, 1992). Aspects of its reproductive and developmental biology have been described (Zhu *et al*., 2007; Long *et al*., 2015). *P. esculenta* has a typical flagellate sperm. Tail formation and head remodeling can be observed during the spermiogenesis of *P. esculenta*. Thus, we selected this species as a model to explore the functions of KIF3A/3B in spermatogenesis.

In this study, 1) full-length KIF3A and KIF3B cDNA were cloned, 2) the expression patterns of *Pe-kif3a/3b* mRNA in various tissue types were evaluated, and 3) FISH and immunofluorescence were performed to examine the functions of *Pe*-KIF3A/3B in sperm head remodeling and tail formation. In addition, detailed descriptions of spermiogenesis in *P. esculenta* were obtained. Our results provide fundamental data for studying the reproductive biology of *P. esculenta*.

2 Materials and Methods

2.1 Preparation of Animals and Sampling

Adult male *Phascolosoma esculenta* used in this experiment was obtained from Xiangshan county of Ningbo (Zhejiang, China). Experimental animals were selected by observing the germ cells in coelomic fluid. The coelomic fluid was stratified with a centrifuge (3000×, 3 min) to purify the spermatid masses. Then, the sperm masses were collected from the top of the liquid. The living individuals were dissected to collect coelomic fluid, the purified spermatid masses, intestine, nephridium, retractor muscle, and body wall. Tissues were stored at −80℃ for RNA extraction. For observation of HE staining, transmission electron microscopy, FISH, and IF, spermatid masses were fixed as detailed in our previous study (Gao *et al*., 2019).

2.2 Light Microscopy (LM) Analyses

Spermatid masses were slightly centrifuged and fixed in Bouin's solution for 24 h at 4℃ and then embedded in paraffin. The paraffin was cut into 7 μm serial sections. The sections were counterstained with hematoxylin and eosin and examined under a light microscope (Olympus BX51).

2.3 Transmission Electron Microscopy (TEM) Analyses

The spermatid masses were fixed in 2.5% glutaraldehyde in cacodylate buffer (pH 7.4) at 4℃ for 2 h and then post-fixed for 1−2 h in 1% osmium tetroxide. After dehydrating in a graded ethanol series and acetone (30%, 50%, 70%, and 90%), cell masses were embedded in epoxy resin. Sections were cut using an ultramicrotome (LKB-α), stained with uranyl acetate for 40 min, and then counterstained with lead citrate (1 min). A transmission electron microscope (JEM-1200EX) was employed to detect the morphological characteristics of the sperm.

2.4 Cloning and Sequencing

Total RNA was extracted from the coelomic cells using Trizol reagent following the instruction of the manufacturer (Takara, Tokyo, Japan). Thereafter, RNA quality was evaluated. The first-strand cDNA was obtained using the PrimerScriptTM RT reagent kit (Takara, Japan). To clone the intermediate fragments of *Pe-kif3a/3b*, we analyzed the amino acid sequences downloaded from the National Center for Biotechnology Information (http://www.ncbi.nlm.nih.gov/, NCBI) and designed degenerate primers by using an online tool (http://blocks.fhcrc.org/blocks/make_blocks.html) Intermediate fragments were cloned under the following PCR conditions: 94℃ for 5 min; 8 cycles of a touch-down program at 94℃ for 30 s, 62℃ for 40 s (0.5 ℃ reduction per cycle), and 72℃ for 40 s; 30 cycles of 94 ℃ for 30 s, 58℃ for 40 s, and 72℃ for 40 s; then 72℃ for

10 min. The amplification products were disposed of following the procedures described by Zhao *et al.* (2017). Specific primers for 3' and 5' RACE were designed using Primer Premier 5.0 software (Premier Biosoft, CA, USA) on the basis of the intermediate chain of *Pe-kif3a/3b*. RACE was performed using the SMARTer^{TM} RACE cDNA Amplification Kit (Clontech, CA, USA) in accordance with the manufacturer's instructions (Primers see Table 1).

Table 1 Primers used in this study

Primer name	Primer sequence (5'–3')	Length	Purpose
KIF3A-F1	GCCCGGACTCCAAGCARHTNGAYGT	25	Cloning
KIF3A-F2	CCAGGATCAACGAGGACCCNAARGAYGC	28	Cloning
KIF3A-F3	CACCGGCAAGACCTTCACNATGGARGG	27	Cloning
KIF3A-F4	GAGCAGCTCAGACATGCGATT	21	Cloning
KIF3A-R1	CAGGTCCTTGATGTACACGCCNACRTCNGG	30	Cloning
KIF3A-R2	GCCATCAGCATGGTCCANACYTTYTT	26	Cloning
KIF3A-R3	ACTGCCCCTTGTGTGCCTT	19	Cloning
KIF3A-R4	GTGTAGGCCACGCACTTCARYTGCCAYTC	29	Cloning
KIF3B-F1	GTGGTGCGGTGCCGNCCNATGAAYG	25	Cloning
KIF3B-F2	CACGCACATCCCCAACAGA	19	Cloning
KIF3B-F3	AGGCACAACTTAGCCAGAGGG	21	Cloning
KIF3B-R1	CACTCGATGGTGATGACGAADATNGCRTG	29	Cloning
KIF3B-R2	CCTCCTCCTCCTCCTCCTCNCCNTCYTC	28	Cloning
KIF3B-R3	CGGACTGCAGCTTGGAGAANARYTTYTT	28	Cloning
3-KIF3A-outer	CTGAGCGAGTGGACATTGAA	20	3' RACE
3-KIF3A-inner	CAAGTCAGAGATGGCAGATA	20	3' RACE
3-KIF3B-outer	TAAACAACAAGTCCCTCATCGC	22	3' RACE
3-KIF3B-inner	GAGCAAAAGAAACGGGAGCG	20	3' RACE
5-KIF3A-outer	CCAGGGTGGACAGGGACAGGTTTA	24	5' RACE
5-KIF3A-inner	CTTCACATACACACCCACATCAGGC	25	5' RACE
5-KIF3B-outer	CAAATACTGTTGGCTTTCTGAGCGGGC	27	5' RACE
5-KIF3B-inner	TTTGCCAGTTCCCGTCTGACCATAGG	26	5' RACE
KIF3A-Real-F	AAGAGCAGCCACATCCCCT	19	Quantitative real-time PCR
KIF3A-Real-R	GGGCATCCTTCGGGTCTT	18	Quantitative real-time PCR
KIF3B-Real-F	TGCCTATGGTCAGACGGGA	19	Quantitative real-time PCR
KIF3B-Real-R	GGTATGATGCTCGCACCAAA	20	Quantitative real-time PCR
GAPDH-F	CCAGAACATCATCCCAGCA	19	Quantitative real-time PCR
GAPDH-R	ACGAACAGGGACACGGAAG	20	Quantitative real-time PCR
KIF3A-probe	GCTTCCGCCTCCCTACATTTC	21	Fluorescence *in situ* hybridization
KIF3B-probe	TCCTTCCTCTTGGTTTTGACTCCC	24	Fluorescence *in situ* hybridization

2.5 Sequence and Phylogenetic Analysis

The information in NCBI (http://www.ncbi.nlm.nih.gov/) was used for sequence analysis. Subcellular localization was predicted on the website http://www.psort.org/. Protein sequences were analyzed and aligned using the Vector NT110 software (Invitrogen, California, USA). A phylogenetic tree was constructed on Mega 5.4. The sequences of KIF3A from human beings and different animals were used in protein alignment and phylogenetic analysis, including *Aplysia californica* [XP_005105009.1], *E. sinensis* [AFP33455.1], *Danio rerio* [NP_001017604.2], *Homo sapiens* [CAJ45482.1], *Xenopus laevis* [NP_001084268.1], *Pteropus Alecto* [ELK03105.1], *Rousettus aegyptiacus* [XP_015973953.1], *Saccoglossus kowalevskii* [XP_006820259.1], *Crassostrea gigas* [EKC19840.1], *Lingula anatine* [XP_013384616.1], *Limulus polyphemus* [XP_013781360.1], and *Drosophila* [NP_523934.1]. Sequences of KIF3B from human beings and different animals were also employed in protein alignment and phylogenetic analysis, including *O. tankahkeei* [AEL16465.1], *D. rerio* [NP_001093615.1], *Mus musculus* [NP_032470.3], *X. laevis* [NP_001081489.1], *A. californica* [XP_005108306.1], *Rattus norvegicus* [NP_001099999.1], *H. sapiens* [NP_004789.1], *E. sinensis* [AIN36848.1], and *Drosophila* [NP_001261726.1]. Protein domains and 3D structure were processed by PROSITE (http://prosite.expasy.org/) and I-TASSER (http://zhanglab.ccmb.med.umich.edu/I-TASSER), respectively.

2.6 Real-Time Quantitative PCR

Specific primers were designed to analyze the expression of *Pe-kif3a/3b* in different tissues. GAPDH served as a positive control (Su *et al.*, 2010). The primers used are listed in Table 1. *Pe-kif3a/3b* expression levels in different tissues were detected by qPCR as described by Zhao *et al.* (2017). The PCR process was 95℃ for 30 s and 40 cycles at 95℃ for 20 s, 60℃ for 20 s, and 72℃ for 20 s. All samples were examined in quintuplicate on the sane plate (n = 5). Data processing and analysis were performed using SPSS 11.0.

2.7 Fluorescence *in Situ* Hybridization

Dual-color FISH was performed to identify the localization of *kif3a*/*3b* mRNA during *P. esculenta* spermiogenesis. The probes were designed by Primer 5.0 and synthesized by Invitrogen (Shanghai, China). The *kif3a* antisense probe was a FITC-labeled 21bp-nucleotide sequence, and

the *kif3b* antisense probe was a Cy3-labeled 24bp-nucleotide sequence (Primers are in Table 1).

Frozen sections of the experimental group and negative control group were incubated with probes (Gao *et al.*, 2019). Then, the sections were observed *via* confocal laser-scanning microscopy (LSM710/780; Carl Zeiss, Germany).

2.8 Antibodies

Polyclonal rabbit anti-KIF3A and polyclonal rat anti-KIF3B were obtained as follows. The fragments in the tail domains of KIF3A (Ala-515 to Glu-687) and KIF3B (Ala-503 to Arg-742) were cloned and ligated into the PEASY-Blunt E1 expression vector (TransGen, Beijing, China), transformed into Trans-T1 competent cells (Fig.1D), and sequenced by Beijing Genomics Institute (Beijing, China). Correct plasmids were extracted using the AxyPre Plasmid Miniprep Kit (Axygen; Beijing, China) and transformed into Transetta (DE3) competent cells to produce the KIF3A-His6 and KIF3B-His6 fusion protein, induced by 1 μmol L^{-1} isopropylthio-β-d-galactoside (Fig.1A). The His-tag Protein Purification Kit was used to purify the fusion protein (Beyotime, Shanghai, China). Protein renaturation was performed similarly to our previous study (Gao *et al.*, 2019) (Fig.1B). Finally, the recombination proteins were sent to Hangzhou Hua'an Biotechnology Co. Ltd. (China) for animal immunization. The specificity of antibodies was detected using Western blot (WB) as previously described (Zhao *et al.*, 2017). The results agreed with the predicted molecular weights (Fig.1C).

The mouse anti-tubulin antibody was purchased from Beyotime Biotechnology to detect the MT (Shanghai, China), and its specificity was analyzed by using WB (data not shown). Horseradish peroxidase (HRP)-conjugated goat anti-rabbit IgG and HRP-conjugated goat anti-rat IgG were purchased from Sangon Biotech (Shanghai, China). Alexa Fluor 488-labeled goat anti-mouse IgG (H+L), Alexa Fluor 488-labeled goat anti-rabbit IgG (H+L), Alexa Fluor 555-labeled goat anti-rabbit IgG (H+L), and Alexa Fluor Cy3-labeled goat anti-rat IgG (H+L) were purchased from Beyotime Biotechnology. The Mito-Tracker Green FM was purchased from Invitrogen (California, USA).

2.9 Immunofluorescence (IF) Analyses

Frozen sections were cut and blocked as in our previ-

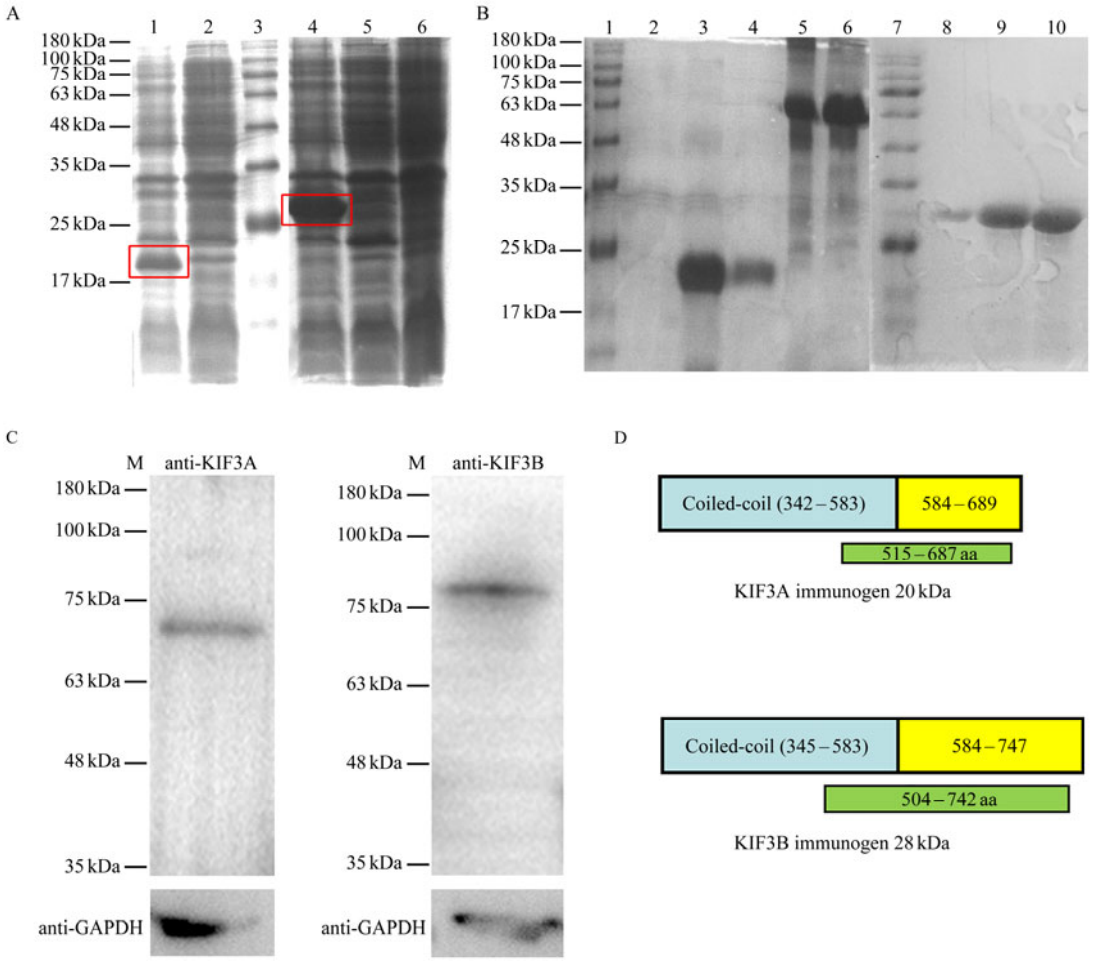

Fig.1 Preparation and validation of antibodies. (A) Expressions of recombinant proteins. The red boxes in Lines 1 and 4 show the expressions of recombinant *Pe*-KIF3A/3B, respectively. The other lines show the control groups. (B) Purification of recombinant proteins. Lines 3 and 4 show the purified recombination *Pe*-KIF3A, Lines 5 and 6 showed the control groups, Lines 9 and 10 show the purified recombination *Pe*-KIF3B. (C) Validation of antibodies. WB was employed to detect the specificity of two polyclonal antibodies. Only a single band appeared in each experimental group and coincided with the predicted molecular weight. (D) Immunogens of *Pe*-KIF3A/3B.

ous work (Zhao *et al*., 2017). Then the frozen sections were incubated with primary antibodies overnight (4℃) and washed with 1×PBS containing 0.1% Triton X-100 (0.1% PBST) in the concentrator (3 times, 15 min per times). After incubation with secondary antibodies for 1 h at room temperature, the sections were washed six times with 0.1% PBST. Finally, the nuclei were stained with DAPI for 5 min. The immunostained tissue sections were observed using a confocal laser-scanning microscope (LSM710/780; Carl Zeiss, Germany). In the negative control, no primary antibody was added.

3 Results

3.1 Morphological Characteristics of Spermatogenic Cells in *P. esculenta*

By observing histological sections, we analyzed the microstructures of spermatogenic cells of *P. esculenta* (Fig.2). According to the size, location, and shapes of the chromatin, germinal cells were divided into four groups: spermatogonium, primary spermatocyte, secondary spermatocyte, and spermatid. Irregular-shaped spermatogonia were located at the near end of the testis with large cell bodies. Their nucleoli were close to the nuclear envelope (Fig.2A). The primary spermatocytes were located at the far-end of the testis with an ovoid-shaped nucleus (Fig.2B). At this stage, small particle-shaped chromatin was randomly distributed in the nucleus. Secondary spermatocytes were mostly located at the far end of the testis, with some floating spermatocytes in the coelomic fluid. Compared with primary spermatocytes, secondary spermatocytes were smaller in size and more regular in shape. In addition, their nuclei were approximately circular, and the chromatin was dispersed into small granules (Fig.2C). Finally, few spermatids were located at the edge of the far-end of the testis, and most cells were free-floating in the coelomic fluid in the form of cell masses (Fig.2D).

The spermiogenesis and spermatid structure in *P. esculenta* were characterized using TEM. In the early stage of spermiogenesis, the newly formed spermatids had round nuclei, the chromatin was not condensed (Figs.2E and 3A), and mitochondria were distributed around the nuclei (Fig.3A). Subsequently, visible proacrosomal vesicles formed by the Golgi apparatus were scattered in the cytoplasm. The initial segment of the flagellum could be observed at this stage (Fig.3B). At the middle stage, the amount of cytoplasm was reduced, as was the cell body size (Fig.2F). Chromatin appeared in patches, and mitochondria began to move to one cell pole. Some proacrosomal vesicles fused into short-flattened acrosomal vesicles (Fig.3C). In the late-stage spermatids, most of the cytoplasm was lost, the karyotheca appeared in irregular shapes, and the chromatin was distributed in the nucleus in the form of compact fine particles (Fig.2G). A mitochondria-rich region appeared. The flagellum and Golgi-centriolar complexes were clearly visible (Fig.3D). The mature spermatid can be divided into two groups, spermatid with mature structure (stored in the coelomic fluid) and physically mature spermatid (stored in the nephridium) (Zhu *et al*., 2007). In the coelomic fluid, the mature spermatids were irregular in shape, the chromatin was highly concentrated, and the cytoplasm could be observed at one cell pole (Figs.2H and 2E). In the nephridium lumen, the sperm exhibited a substantial shape change; a cap-shaped acrosome appeared, and the nucleus exhibited a pear shape. A short midpiece and a slender flagellum with a typical '9+2' structure could be observed (Figs.3I and 3F).

3.2 cDNA Sequence and Structural Analysis of *Pe-kif3a* and *Pe-kif3b*

The *Pe-kif3a* (GenBanK number: KY411164) cDNA sequence was 2500 bp, with a 293 bp 3' UTR (untranslated region), a 137 bp 5' UTR, and a 2070 bp open reading frame (ORF). The polypeptide had a predicted molecular mass of 78.1 kDa and a theoretical isoelectric point of 6.38. *Pe-*

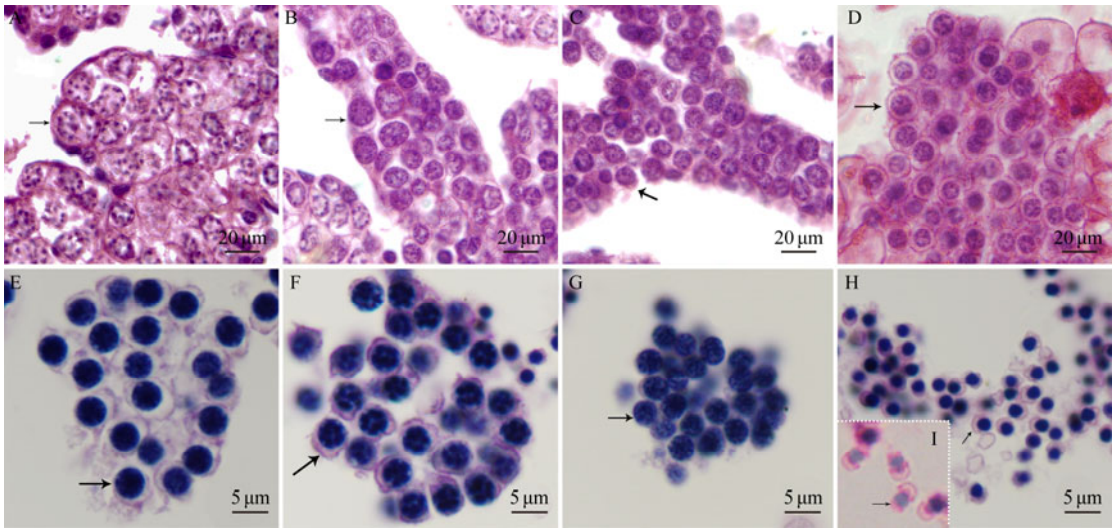

Fig.2 Microstructural characteristics of spermatogenesis in *P. esculenta*. Microstructures of spermatogenetic cells were analyzed by observing histological sections with HE staining: (A) spermatogonium, (B) primary spermatocyte, (C) secondary spermatocyte, (D) spermatid, (E) early spermatid, (F) middle spermatid, (G) late spermatid, (H) sperm in coelomic fluid, and (I) sperm in nephridium lumen. The arrows indicate spermatids in the corresponding stage.

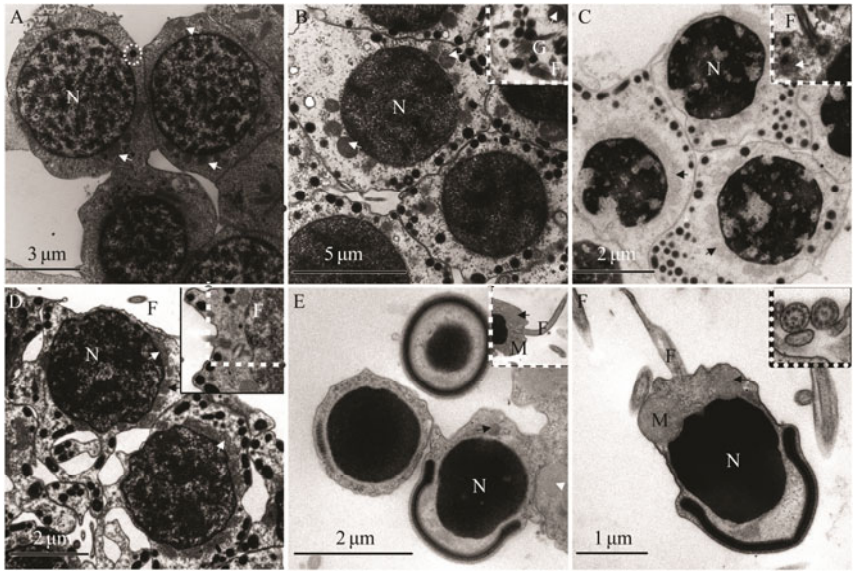

Fig.3 Ultrastructural characteristics of spermiogenesis in *P. esculenta*. TEM was employed to analyze the ultrastructures of spermiogenesis: (A) newly formed spermatid, (B) early spermatid, (C) middle spermatids, (D) late spermatids, (E) sperm in coelomic fluid, and (F) sperm in nephridium lumen. N, nucleus; M, mitochondrion; F, flagellum; G, Golgi apparatus. The dotted circles indicate the proacrosomal vesicles. The triangle indicates the abandoned cytoplasm. The arrows (black and white) indicate the mitochondria.

```
1 agagtacatggggattcccaaagcaaaatggcagccaggttttgacagtcgttattcata
61 ttgagatggagaactgcattttgcccccagttgtacatttgaattcacctagatagagaa
1                M P G K K D S D N V R V V V R
121 aaaaatatttcagcaccATGCCAGGGAAGAAGGACTCTGACAATGTGCGGGTGGTGGTCC
16   C R P M N E K E K A S G C K M T V K I D
181 GCTGTCGACCCATGAATGAGAAAGAAAAGGCCTCTGGTTGTAAGATGACCGTCAAGATTG
36   G V Q G T T T V T N P H A T H G E P P K
241 ATGGAGTGCAGGGAACAACAACAGTAACCAACCCTCATGCAACCCATGGGGAGCCCCCCA
56   T F T F D T V F D T D C K Q V D V Y N K
301 AGACTTTCACATTCGACACAGTTTTTGACACAGATTGCAAGCAAGTTGATGTTTACAACA
76   V A R P I V D F V L E G Y N G T I F A Y
361 AAGTTGCCCGCCCAATTGTTGACTTTGTATTGGAGGGTTACAATGGTACCATCTTTGCCT
96   G Q T G T G K T F T M E G V R T V P E L
421 ATGGTCAGACTGGAACAGGGAAGACGTTTACCATGGAGGGAGTACGGACGGTCCCCGAGC
116  R G I I P N S F A H I F G H I A K A E G
481 TGCGTGGAATCATACCCAACTCCTTTGCACACATTTTTGGTCACATTGCAAAAGCTGAAG
136  D T R F L V R V S Y L E I Y N E E V R D
541 GTGATACAAGATTCCTGGTGCGAGTTTCATATCTTGAAATCTACAACGAAGAGGTACGAG
156  L L G K D Q N Q R L E V K E R P D V G V
601 ATCTACTGGGAAAGGACCAGAACCAGCGACTTGAGGTAAAAGAAAGGCCTGATGTGGGTG
176  Y V K D L S A F V V N N A D D M D R I M
661 TGTATGTGAAGGATTTGTCTGCCTTTGTGGTGAATAATGCTGATGACATGGACAGAATAA
196  T L G N K N R A V G A T N M N E Q S S R
721 TGACACTTGGAAACAAAAACAGAGCTGTTGGTGCTACAAACATGAATGAGCAAAGCTCAA
216  S H A I F T V T I E C S E K G P D G K Q
781 GGTCCCATGCGATATTTACTGTCACTATTGAGTGTAGTGAAAAAGGTCCCGATGGGAAAC
236  H V R V G K L H L V D L A G S E R Q S K
841 AACACGTGCGAGTAGGAAAACTCCATCTGGTGGACTTGGCTGGTTCAGAGAGGCAGTCAA
256  T G A T G Q R L K E A T K I N L S L S T
901 AAACTGGAGCTACAGGACAGCGGCTAAAAGAGGCTACGAAGATAAACCTGTCCCTGTCCA
276  L G N V I S A L V D G K S S H I P Y R N
961 CCCTGGGCAATGTGATCTCAGCTCTGGTCGATGGCAAGAGCAGCCACATCCCCTACAGGA
296  S K L T R L L Q D S L G G N S K T V M V
1021 ACTCCAAGCTCACACGTCTGCTGCAAGACTCACTGGGCGGCAACTCCAAAACTGTCATGG
316  A N F G P A D Y N Y D E T I S T L R Y A
1081 TTGCTAATTTCGGGCCTGCAGACTACAACTATGATGAAACCATCAGCACCCTGCGCTATG
336  N R A K N I K N N A R I N E D P K D A L
1141 CCAACCGTGCCAAGAACATCAAGAACAATGCAAGGATCAACGAAGACCCGAAGGATGCCC
356  L R Q F Q K E I E E L K K R L E D G D Y
1201 TGCTGCGGCAGTTTCAAAAGGAGATCGAAGAGCTCAAGAAGAGGCTTGAGGATGGAGACT

376  S G S E E G S T E E D E E E G P D G S P
1261 ACTCAGGGTCCGAGGAAGGCTCTACAGAGGAAGATGAGGAAGAGGGACCAGATGGTAGCC
396  K R H R R K K K G A K I S K E R M V A I
1321 CCAAGAGACACAGGAGAAAAAAAAAGGGAGCAAAGATTTCGAAGGAGCGCATGGTGGCCA
416  Q A Q I E A D R R K L E Q Q K D M E E E
1381 TCCAAGCTCAGATTGAGGCTGACCGCAGGAAGCTGGAACAGCAGAAGGATATGGAGGAGG
436  E K R R V E Q D L A S K E S E L Q Q A K
1441 AAGAGAAACGCAGAGTGGAGCAGGACCTTGCCTCCAAAGAGTCTGAGCTGCAGCAGGCCA
456  D E Q D Q L A Q K L A A I E K K I I V G
1501 AAGATGAGCAGGACCAACTGGCCCAGAAGTTGGCTGCCATTGAGAAGAAGATCATCGTGG
476  G E N L L E K A E E Q E R L L E E S K Q
1561 GTGGTGAAAACCTGCTGGAGAAGGCCGAGGAACAGGAGCGCCTCCTTGAGGAGAGTAAGC
496  E L D K N K Q R E E D L R R A L Q E K E
1621 AGGAGTTGGACAAGAACAAGCAGAGGGAGGAGGACCTGCGGCGCGCTCTGCAGGAGAAAG
516  A E R V D I E E E K Y S S L Q E E A T G K
1681 AGGCTGAGCGAGTGGACATTGAAGAAAAGTATTCCAGCCTGCAGGAAGAAGCCACTGGCA
536  T R K L K K V W T M L M Q A K S E M A D
1741 AAACCCGCAAGTTGAAGAAAGTCTGGACAATGCTCATGCAGGCCAAGTCAGAGATGGCAG
556  I Q Q E H Q R E M E G L L E N V R Q L S
1801 ATATACAGCAGGAGCATCAGCGGGAGATGGAGGGTCTGCTGGAGAATGTTCGACAGCTGA
576  R E L R L Q T L I I D N F I P P E Y Q E
1861 GCCGAGAGCTGCGGCTGCAGACGCTCATCATTGACAATTTCATCCCACCAGAATACCAGG
596  M I E Q Y V H W N E D I G E W Q L K C V
1921 AGATGATAGAACAGTACGTGCATTGGAATGAGGATATTGGAGAATGGCAACTGAAGTGTG
616  A Y T G N N M R K Q T P L P D K D R E K
1981 TGGCATATACAGGCAACAATATGCGCAAGCAGACCCCACTGCCAGACAAGGACAGAGAAA
636  Y Q E P D L S N V Y L A Y T A E G A E M
2041 AGTACCAAGAACCAGACCTTTCTAATGTGTACCTGGCGTACACAGCAGAAGGAGCTGAGA
656  A M K Q K S G K G K G G R P K N G G G R
2101 TGGCCATGAAGCAAAAGTCTGGCAAGGGTAAAGGCGGCCGACCCAAGAACGGTGGTGGGC
676  P K T G K K K C R E A E A D *
2161 GGCCCAAGACAGGCAAGAAGAAATGTAGGGAGGCGGAAGCTGACTAGcacatcatgacca
2221 ttgtattcagctgtcatggcatttatttgaattctcagacaaaacactccatttttgtgt
2281 ttgtgaatggtcttattgtgatatttgtttccttgtgtaagtcatgtcattctgccaata
2341 tagatagggtggaaaacatgaaatgtcattcatgaaaaaatattgctttctataaagcct
2401 aaatatgattaaaaagacaaattggtaaatgattaaaaattccacattggggtataatta
2461 taaactacatatatgaaaagcttgattgccaaaaaaaaaa
```

Fig.4a *Pe-Kif3a* full-length cDNA and amino acid sequence. The initiation codon (ATG) and termination codon (TGA) are set to yellow and blue, respectively. The red circles show the ATP bind sites, and the black boxes show the MT-binding sites. The blue line shows the neck linker.

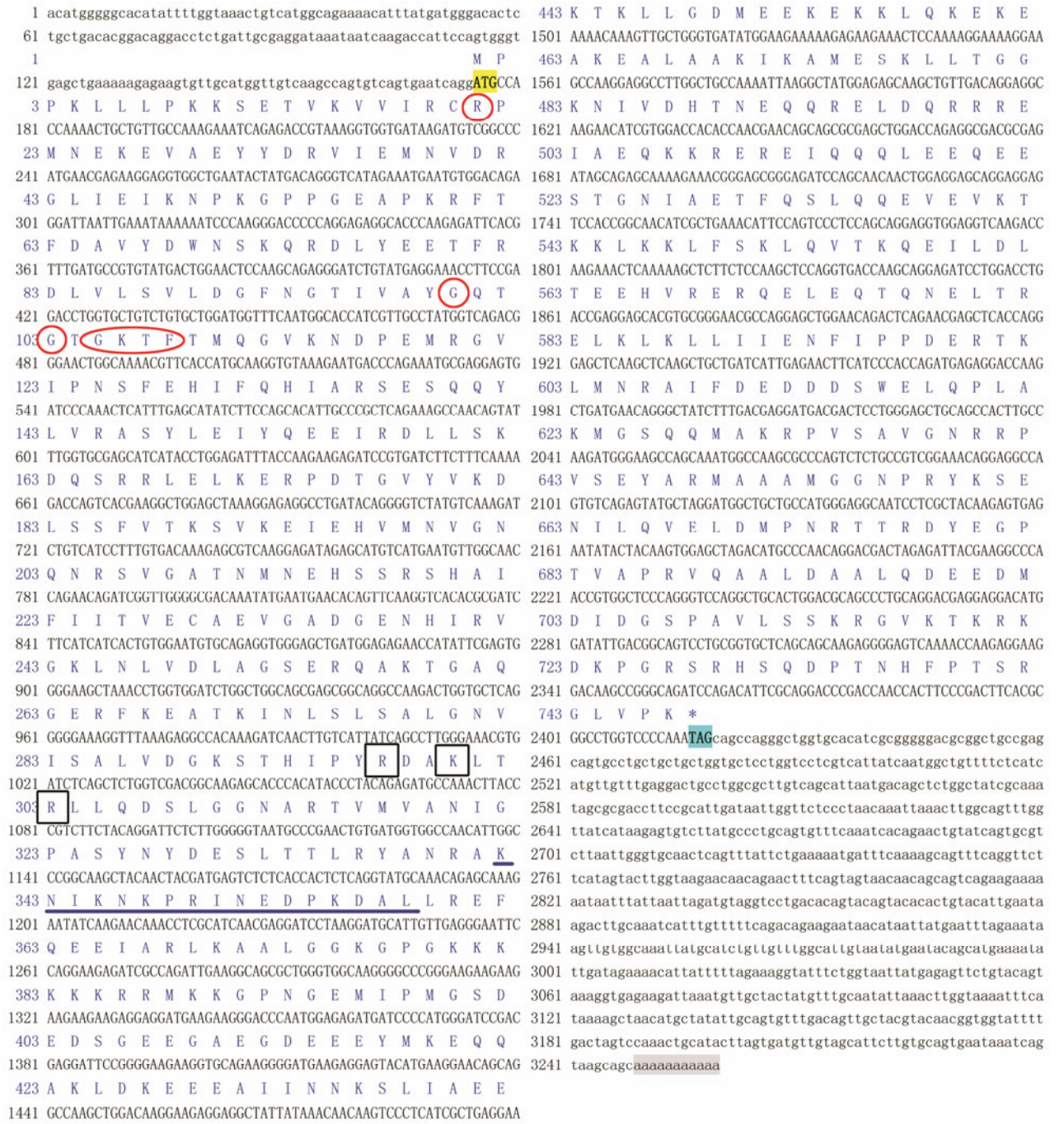

Fig.4b Same as Fig.4a but for *Pe-Kif3b* full-length cDNA and amino acid sequence.

KIF3A had a conserved central catalytic motor domain (8–341 aa) containing eight ATP-binding sites (17-Arg, 96-Gly, 99-Gly, 101-Gly, 102-Lys, 103-Thr, 104-Phe, and 246-Asp) and three MT-binding sites (294-Arg, 297-Lys, and 300-Arg). The neck linker (KNIKNKPRINEDPKDAL) could connect the head domain and the coiled–coil domain; it was located between residues 339 and 355. Moreover, we detected bipartite NLS motifs (KRHRRKKK, PKTGKKK) and bipartite site RRKLEQQKDMEEEEKRRV (Fig.4a).

The full-length *Pe-kif3b* was 3259 bp (GenBanK number: KY411165), consisting of an 841-bp 3' UTR, a 174 bp 5' UTR, and a 2244 bp ORF. The polypeptide had a predicted molecular mass of 84.7 kDa and a theoretical isoelectric point of 7.64. It also had ATP-binding sites (21-Arg, 100-Gly, 103-Gly, 105-Gly, 106-Lys, 107-Thr, 108-Phe, and 249-Asp) and MT-binding sites (297-Arg, 300-Lys, and 303-Arg) in the motor domain (11–344 aa). The neck linker was located between residues 342 and 357. *Pe*-KIF3B may be located in the nucleus, nucleolus, cytoplasm, and mitochondria. In addition, we detected an NLS motif (PGKK KKKKRR) (Fig.4b).

The predicted secondary structure revealed that *Pe*-KIF3A and *Pe*-KIF3B could be divided into three domains (Fig.5A). *Pe*-KIF3A was composed of a head at the N-terminal end, a helical stalk (342–583 aa) and a tail (584–689 aa) at the C-terminal end. *Pe*-KIF3B was also composed of a head (1–344 aa), a helical stalk (345–583 aa), and a tail (584–747 aa). The head was the catalytic

core responsible for ATP-hydrolysis and MT binding. The 3D structural predictions for *Pe*-KIF3A and *Pe*-KIF3B were similar, including a globular head, a coiled-coil neck, and a globular tail (Fig.5B).

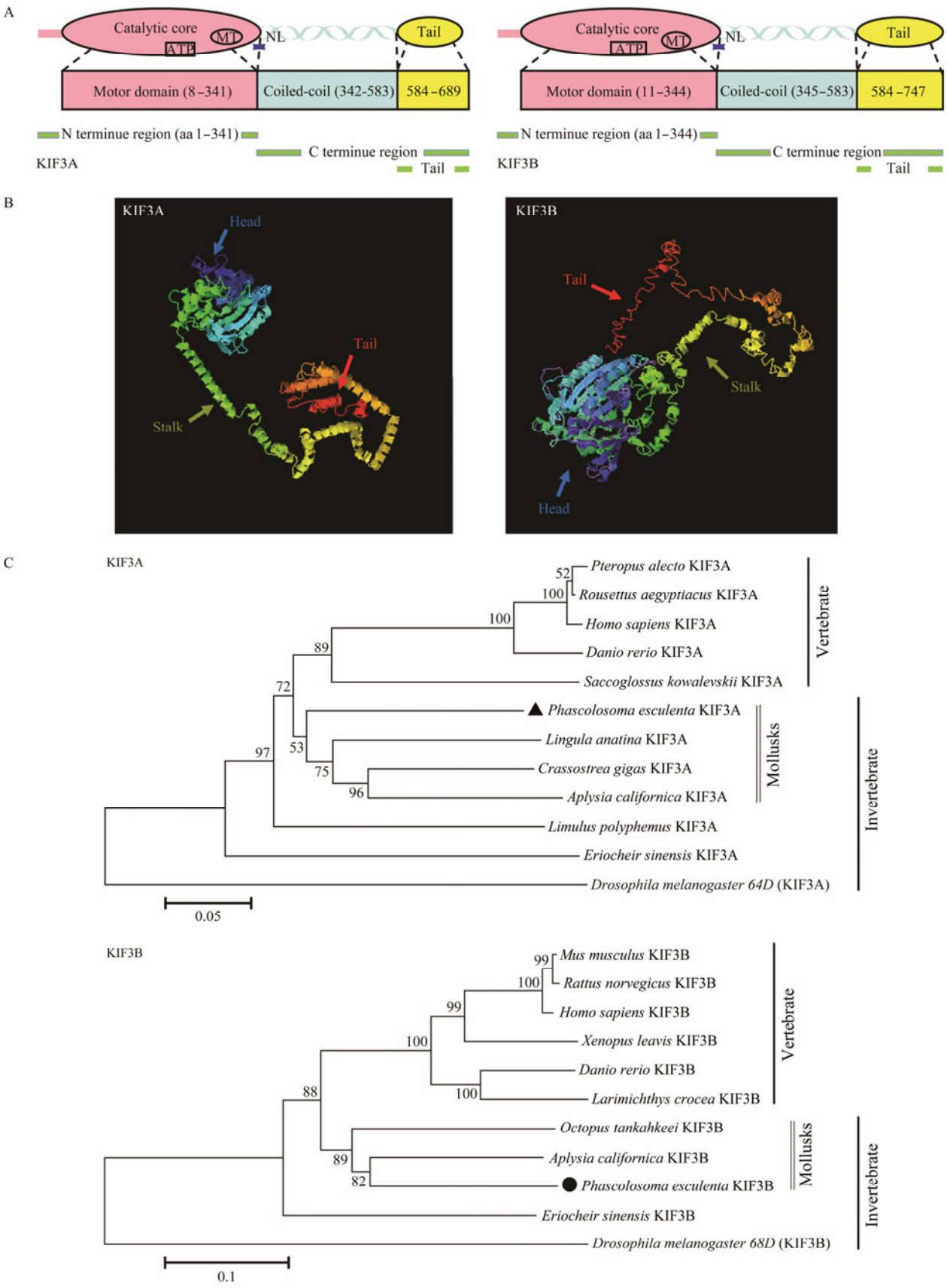

Fig.5 Structural prediction of *Pe*-KIF3A/3B proteins. A, Putative diagram of *Pe*-KIF3A/3B secondary structure; B, Putative diagram of *Pe*-KIF3A/3B tertiary structure; C, Phylogenetic analysis of *Pe*-KIF3A/3B. To construct the phylogenetic tree (NJ method), Mega 5.1 software was employed. Scale bar: 0.1 of the branch length value.

3.3 Sequence Alignment and Phylogenetic Analysis

The sequence of *Pe*-KIF3A shared 77%, 57.3%, 66.6%, 71.8%, 69.2%, and 71.2% identity with the homologous proteins in *A. californica*, *Drosophila melanogaster*, *E. sinensis*, *D. rerio*, *H. sapiens*, and *X. laevis*, respectively. *Pe*-KIF3A had high homology with sequences in other species, especially in its putative motor domain. In addition, the MT-binding sequence (YNEEVRDLL) and ATP-binding sequence (AYGQTGTGKT, SSRSH, and LAGSE) (Fig.6A) were shared among species. The identities of KIF3B between *P. esculenta* and *O. tankahkeei*, *D. rerio*, *M. musculus*, *X. laevis*, and *A. californica* were 70.3%, 66.0%, 69.1%, 66.9%, and 73.5%, respectively. The sequence of Pe-KIF3B also shared the MT-binding sequence (HLPYRDSKLTRLL) and ATP-binding sequence (VVV RCRP, NGTIFA, GQTGTGKT and DGENHIRVGKLNL VDLAGSERQ) with those of other species (Fig.6B). *Pe*-KIF3A/3B showed low conservation in non-motor domains.

We generated a phylogenetic tree by the neighbor-joining (NJ) method to evaluate *Pe*-KIF3A and *Pe*-KIF3B in an evolutionary framework. *Pe*-KIF3A shared the highest similarity with homologs in the mollusks *C. gigas* and *L. anatine*, and *Pe*-KIF3B shared the highest similarity with homologs in the mollusks *A. californica* and *O. tankahkeei* (Fig.5C).

3.4 Relative Abundance of *Pe-kif3a/3b* mRNA

The purified spermatid mass, intestine, nephridium, retractor muscle, and body wall were obtained from adult worms and quantified by real-time quantitative PCR to examine the relative abundances of *kif3a* and *kif3b* transcripts in *P. esculenta*. *Pe-kif3a/3b* mRNAs were detected in all tissues assayed (Fig.7). The sperm masses had the highest abundances of *Pe-kif3a/3b*, suggesting that these loci play crucial roles in *P. esculenta*, especially in spermiogenesis.

3.5 Dynamic Expression Patterns of *Pe-kif3a*/*3b* mRNA During Spermiogenesis

FISH was employed to precisely determine the temporal and spatial expression patterns of *Pe-kif3a/3b* during spermiogenesis in *P. esculenta*. Negative controls with sense probes were used to detect the specificity of fluorescence

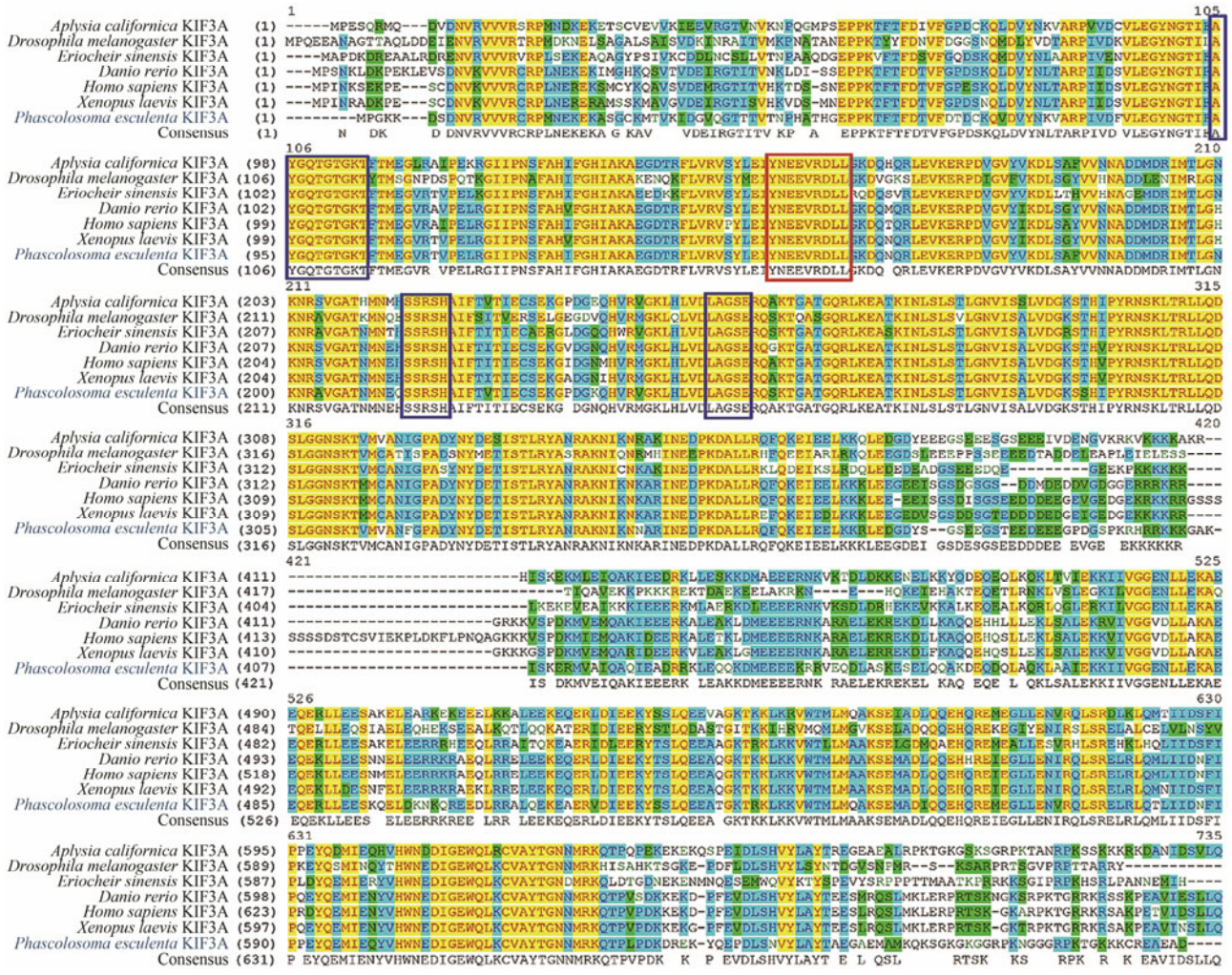

Fig.6A Multiple sequence alignment of KIF3A homologous proteins. The blue boxes indicate the putative ATP-binding sites (AYGQTGTGKT, SSRSH, and LAGSE). The red boxes indicate the putative microtubule binding sites (YNEE VRDLL).

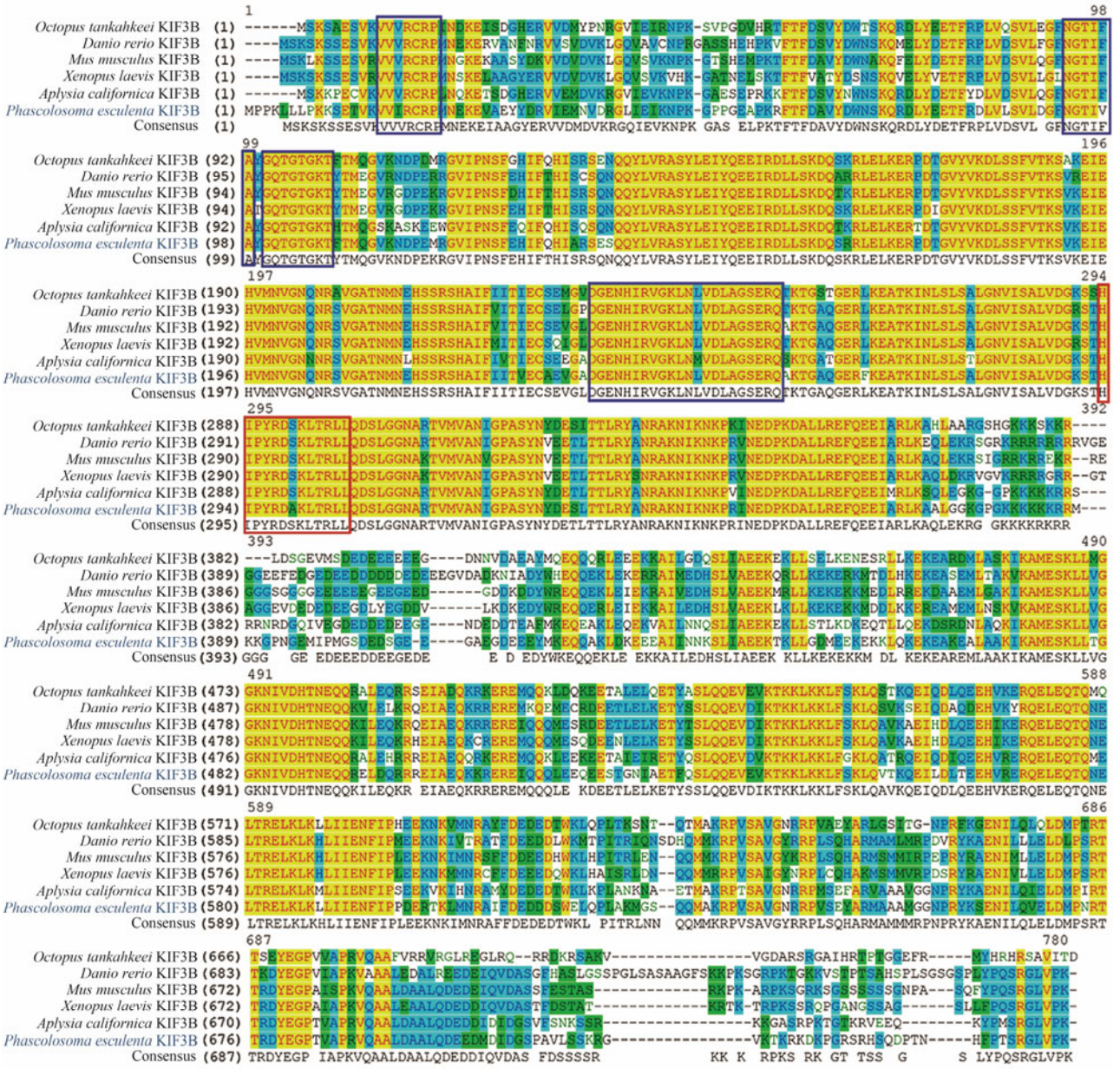

Fig.6B Multiple sequence alignment of KIF3B homologous proteins. The blue boxes indicate the putative ATP-binding sites (VVVRCRP, NGTIFA, GQTGTGKT, and DGENHIRVGKLNLVDLAGSERQ). The red boxes indicate the putative microtubule binding sites (HLPYRDSKLTRLL).

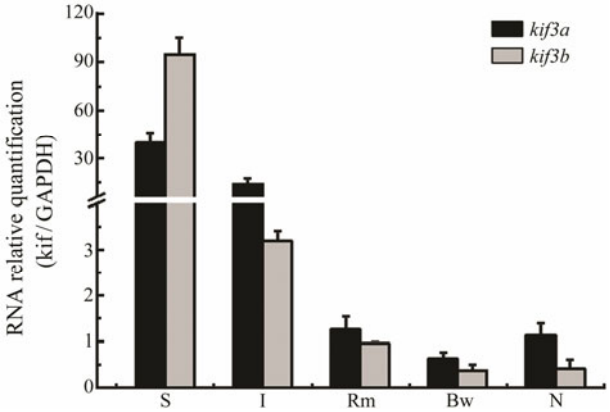

Fig.7 Relative abundance of *Pe-kif3a/3b* mRNA in different tissues. Relative abundance levels of *Pe-kif3a* (black bars) and *Pe-kif3b* (gray bars) in different tissues were detected by qPCR. *Pe-kif3a* and *Pe-kif3b* show the highest expression levels in spermatid mass. S, spermatid mass; I, intestine; N, nephridium; Rm, retractor muscle; Bw, body wall. All samples were examined in quintuplicate on the same plate ($n=5$).

signals (data not shown). The expression patterns of the two genes were similar. In the early stage of spermatids, *Pe-kif3a* and *Pe-kif3b* exhibited low expression levels, and signals were sporadically distributed in the cytoplasm (Figs.8A1–A4). In the middle stage of spermatids, *Pe-kif3a* and *Pe-kif3b* exhibited remarkably elevated expression levels distributed evenly throughout the cytoplasm (Figs.8B1–B4). In the late stage of spermatids, the expression patterns of *Pe-kif3a* and *Pe-kif3b* were restricted, with dense signals at one cell (Figs.8C1–C4) pole. In mature sperm, *kif3a* and *kif3b* signals were intense in the subacrosomal space and tail midpiece (Figs.8D1–D4).

3.6 Co-Localization of *Pe*-KIF3A/3B with MTs During *P. esculenta* Spermiogenesis

Using immunofluorescence, we analyzed the protein expression characteristics of *Pe*-KIF3A, *Pe*-KIF3B, and MTs (Figs.9, 10). In early spermatids, each of the three proteins exhibited weak expression in the cytoplasm, and *Pe*-KIF3A/3B co-localized with MTs (Figs.9, 10A1–A4). In intermediate spermatids, the signals of MTs and *Pe*-KIF3A/3B were enhanced and co-localized in the cytoplasm (Figs.9, 10B1–B4). In late spermatids, the MTs signals were dense and were tightly packed in the nucleus, whereas *Pe*-KIF3A/3B were detected in the karyotheca at one pole (Figs.9, 10C1–C4). In the sperm, the expression levels of both proteins were remarkably reduced. *Pe*-KIF3A/3B signals were detected in the midpiece and flagellum, and the MT signals were co-localized with KIF3A/B in the flagellum (Figs.9, 10D1–D4).

3.7 *Pe*-KIF3A/3B Mediated the Migration of Mitochondria During *P. esculenta* Spermiogenesis

Immunofluorescence was performed to detect whether KIF3A/3B serve mitochondria-related functions during *P. esculenta* spermiogenesis. Notably, *Pe*-KIF3A and *Pe*-KIF3B co-localized with mitochondria. The co-localized signals could be observed during spermiogenesis (Figs.11, 12). In early spermatids, few mitochondria and *Pe*-KIF3A/3B were evenly distributed in the cytoplasm. (Figs.11, 12A1–A4). In the middle spermatids, the co-localization increased (Figs.11, 12B1–B4). The migration of mitochondria was initially detected in the middle spermatids, and the signals were located in the postnuclear cytoplasm (Figs.11, 12 C1–C4). In addition, co-localization was detected in the midpiece of the sperm tail (Figs.11, 12D1–D4).

3.8 Co-Localization of *Pe*-KIF3A with *Pe*-KIF3B During Spermiogenesis

Immunofluorescence showed that *Pe*-KIF3A co-localized with *Pe*-KIF3B at all stages of *P. esculenta* spermiogenesis (Fig.13). In the early and middle stages, *Pe*-KIF3A and *Pe*-KIF3B were both localized around the nucleus. In the late spermatids, both proteins were localized along one side of the nucleus. In the mature sperm, the co-localized signals were observed at the midpiece of the tails. The co-localization of *Pe*-KIF3A and *Pe*-KIF3B implied the heterodimerization of the two proteins as well as their potential functions in spermiogenesis. These results provide a basis for a model of the distribution of KIF3A and KIF3B during spermiogenesis in *P. esculenta* (Fig.14a).

4 Discussion

In this study, we observed several noteworthy morphological changes during *P. esculenta* spermiogenesis. 1) We observed a decrease in cell size. In our previous study, we found that the cytoplasm forms a pseudopod-like protuberance in middle-stage spermatids, which is later lost by exocytosis, leading to a decrease in cell size (Long *et al*., 2015; Gao *et al*., 2019). In mammals, exocytosis is regulated by MT-dependent IFT *via* Kinesin II (Finetti *et al*., 2009). However, whether *Pe*-KIF3A/3B functions in a similar manner during *P. esculenta* spermiogenesis is unclear. 2) With respect to sperm head deformation, we observed acrosome biogenesis and nuclear reshaping. MTs likely facilitate sperm head deformation in mice (O' Donnell and O' Bryan, 2014). We found that MTs surrounded the nuclei during these processes (Figs.9, 10). 3) The enflagellation and migration of mitochondria were observed. Overall, several significant morphological changes were observed during spermiogenesis in *P. esculenta*, and these changes were associated with MTs and Kinesin3A/3B. These findings are discussed in detail below.

4.1 Bioinformatics and Expression Analyses of *Pe-kif3a/3b*

KIF3A and KIF3B can be divided into the N-terminal motor domain, coiled-coil domain, and C-terminal tail domain (De Cuevas *et al*., 1992). Using online prediction tools, we found that Pe-KIF3A/3B had these structures, including highly conserved motor domains containing ATPase and MT-binding sites. The tail domain can interact with other subunits of holoenzymes and cargoes (Miki *et al*., 2005; Ma *et al*., 2017). Coiled-coil domains act as bridges for interactions between KIF3A and KIF3B (Yamazaki *et al*., 1994; Yamazaki *et al*., 1996; Chana *et al*., 2005; Guzik-Lendrum *et al*., 2015; Mu *et al*., 2019), enabling hetero-dimerization (Rashid *et al*., 1995). In the present study, the coiled-coil domains in *Pe*-KIF3A/3B were relatively conserved, suggesting that *Pe*-KIF3A/3B is also heterodimerized in *P. esculenta*.

mRNA expression patterns are usually associated with functions of the proteins. *Kif3a/3b* mRNAs are found in various tissues and organs among species (Henson *et al*., 1997; Wang *et al*., 2010; Hu *et al*., 2012; Lu *et al*., 2014; Zhao *et al*., 2017). In our study, *Pe-kif3a/3b* mRNAs were detected in all tissues assayed (Fig.7). The highest transcript abundances were found in sperm masses, suggesting their crucial roles in *P. esculenta*, especially in spermiogenesis. Using FISH, we observed *Pe-kif3a/3b* signals at all stages of spermiogenesis but at low levels in the newly formed spermatid (Fig.8). In middle-stage spermatid, *Pe-kif3a/3b* expression levels reached a peak, and various morphological changes were observed by TEM (as shown in Fig.2), including chromatin condensation, enflagellation, mitochondria migration, and increased proacrosomal

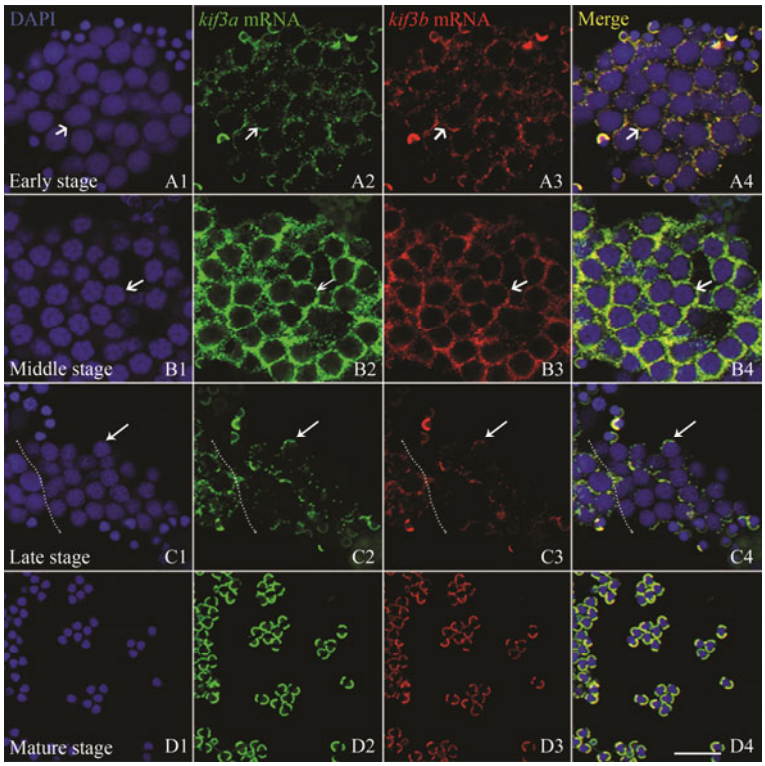

Fig.8 Dynamic expression pattern of *Pe-kif3a/3b* during spermiogenesis. FISH was employed to analyze the expression pattern of *Pe-kif3a* (green) and *Pe-kif3b* (Red). DAPI shows the nuclei (blue). A1–A4 show the early spermatids. *Pe-kif3a/3b* were weakly expressed in the perinuclear cytoplasm. B1–B4 show the middle spermatids. The expression level of *Pe-kif3a/3b* reached a peak. C1–C4 show the late spermatids. The white arrow shows the signals, which were concentrated and located at one side of the cell. D1–D4 show the mature sperm. The signals could be detected in the midpiece and subacrosomal space. The scale bar is 10 μm.

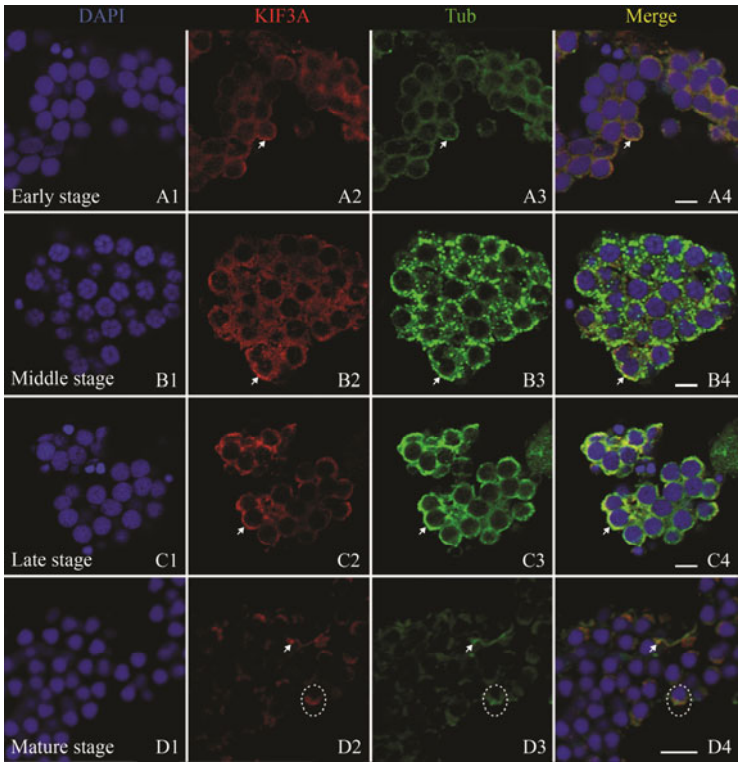

Fig.9 Localization of *Pe*-KIF3A and tubulin during *P. esculenta* spermiogenesis. IF assay shows the localization of *Pe*-KIF3A and tubulin. The tubulin signals (green) were co-localized with *Pe*-KIF3A (red) during all stages of spermiogenesis. DAPI (blue) shows the nucleus. The arrows and dotted circles show the signals. A1–A4 show the early spermatids. *Pe*-KIF3A co-localized with tubulin in the perinuclear cytoplasm at a low level. B1–B4 show the middle spermatids. C1–C4 show the late spermatids. Co-localization of *Pe*-KIF3A and tubulin could be observed in the cytoplasm near the nuclear membrane. D1–D4 show the mature sperm. Signals co-localized at the midpiece. The scale bar is 10 μm.

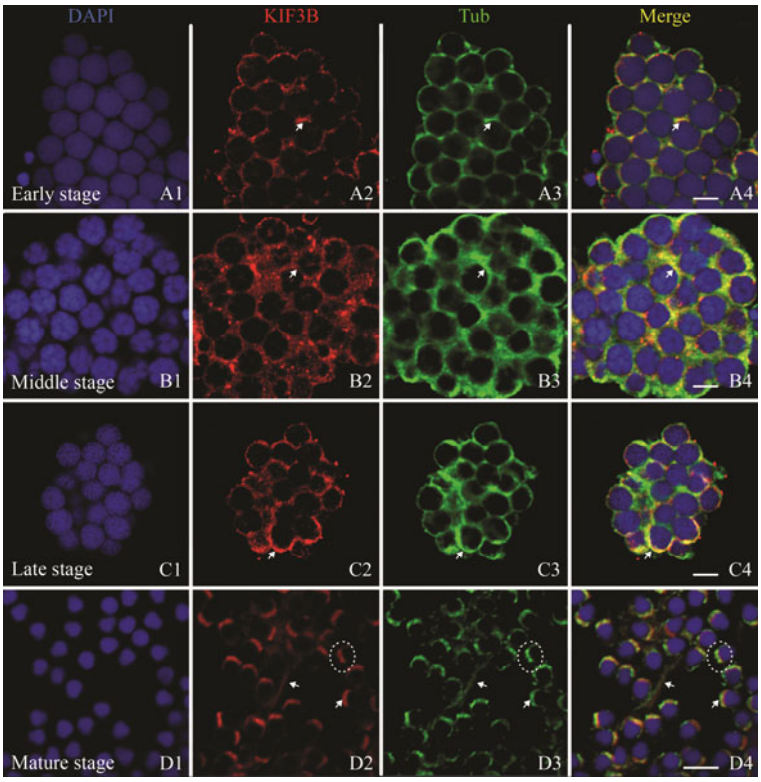

Fig.10 Localization of *Pe*-KIF3B and tubulin during *P. esculenta* spermiogenesis. IF assay shows the localization of *Pe*-KIF3B (red) and tubulin (green). DAPI (blue) shows the nucleus. The arrows and dotted circles show the signals. A1–A4 show the early spermatids. B1–B4 show the middle spermatids. C1–C4 show the late spermatids. D1–D4 show the mature sperm. The scale bar is 10 μm. The co-localization of *Pe*-KIF3B and tubulin shares the same pattern as *Pe*-KIF3A and tubulin.

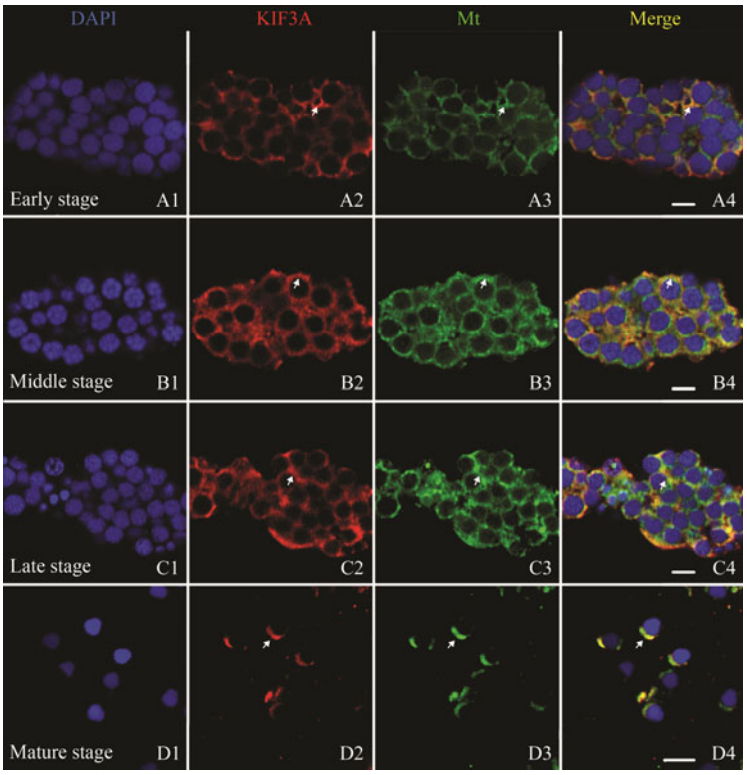

Fig.11 Localization of *Pe*-KIF3A and Mito-tracker during *P. esculenta* spermiogenesis. IF was employed to analyze the co-localization of *Pe*-KIF3A and mitochondria. DAPI (blue) shows the nucleus. Mito-tracker signals (green) were co-localized with *Pe*-KIF3A (red) during all stages. A1–A4 show the early spermatids. *Pe*-KIF3A co-localized with mitochondria in the perinuclear cytoplasm. B1–B4 show the middle spermatids. The co-localized signals were detected in the cytoplasm. C1–C4 show the late spermatids. Co-localization of *Pe*-KIF3A and mitochondria could be observed on one side of the spermatid. D1–D4 show the mature sperm. Notably, they were co-localized at the midpiece. The scale bar is 10 μm.

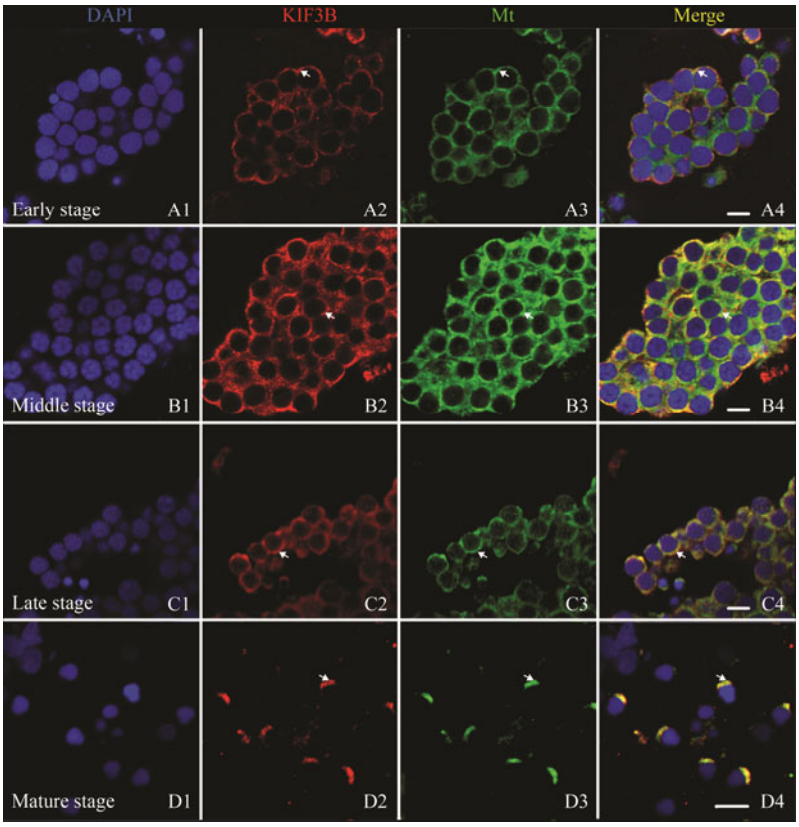

Fig.12 Localization of *Pe*-KIF3B and Mito-tracker during *P. esculenta* spermiogenesis. DAPI (blue) shows the nucleus. Mito-tracker signals (green) were co-localized with *Pe*-KIF3B (red). A1–A4 show the early spermatids. B1–B4 show the middle spermatids. C1–C4 show the late spermatids. D1–D4 show the mature sperm. The scale bar is 10 μm.

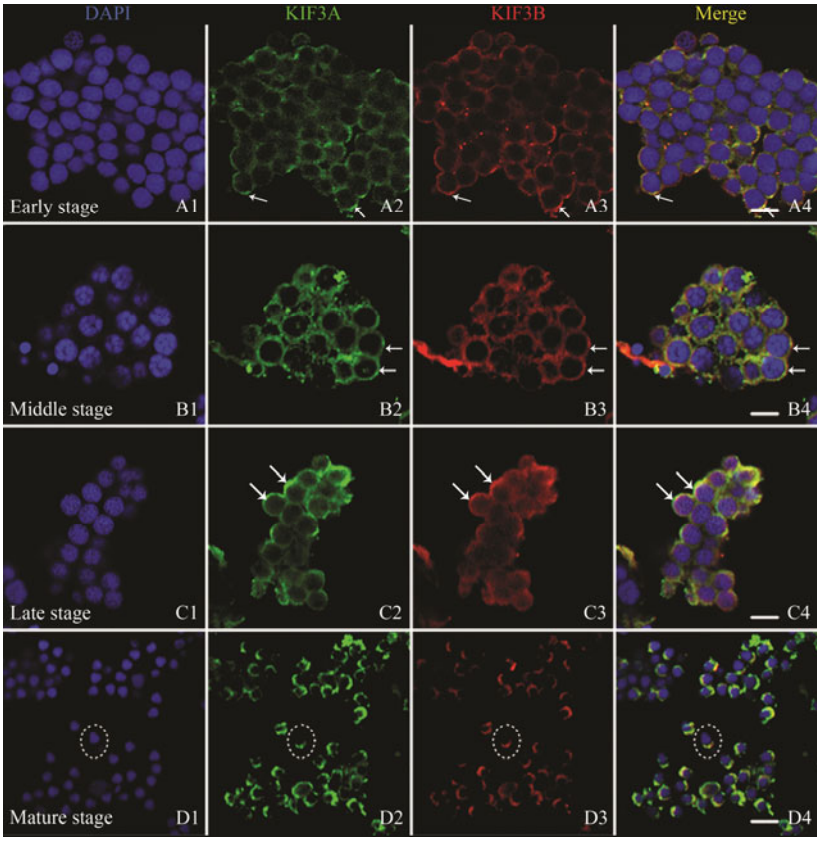

Fig.13 Co-localization of *Pe*-KIF3A with *Pe*-KIF3B during *P. esculenta* spermiogenesis. IF assay shows the co-localization of *Pe*-KIF3A (green) and *Pe*-KIF3B (red). A1–A4 show the early spermatids. B1–B4 show the middle spermatids. C1–C4 show the late spermatids. D1–D4 show the mature sperm. *Pe*-KIF3A always co-localized with *Pe*-KIF3B. Co-localization indicates the heterodimerization of the two proteins. The scale bar is 10 μm.

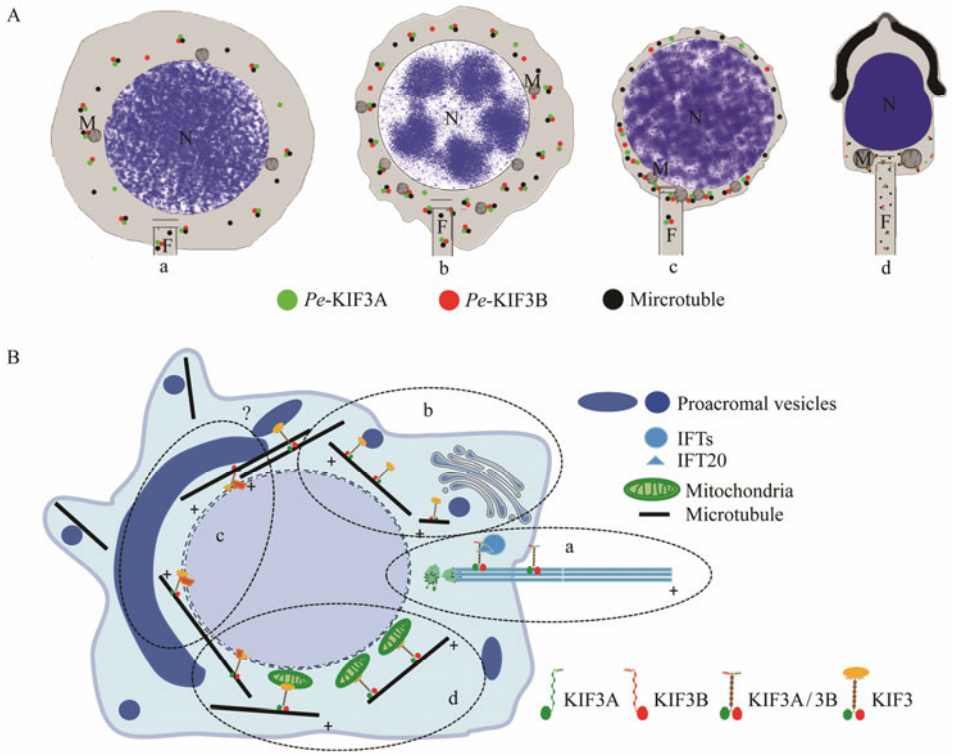

Fig.14 A, Model of the dynamic distribution of *Pe*-KIF3A/3B during spermiogenesis in *P. esculenta*. M, mitochondria; N, nucleus; F, flagellum. (a), in the early stage, *Pe*-KIF3A/3B were sporadically distributed in the cytoplasm; (b), in the middle stage, *Pe*-KIF3A/3B exhibited remarkably elevated expression levels; (c), in the late stage, the expression patterns of *Pe*-KIF3A/3B were restricted; (d), in mature sperm, *Pe*-KIF3A/3B signals were intense in the tail midpiece. The scale bar is 10 μm. B, Model of *Pe*-KIF3A/3B putative functions in *P. esculenta* spermiogenesis. Based on our results, we suggested that (a) *Pe*-KIF3A/3B participate in enflagellation and flagellar maintenance through IFT; (b) *Pe*-KIF3A/3B may transport the acrosomal vesicles from the Golgi apparatus during acrosome biogenesis; (c) *Pe*-KIF3A/3B might participate in sperm head remodeling; (d) in addition, the two proteins are involved in mediating mitochondrial behavior during midpiece formation.

vesicles (Long *et al*., 2015). These results implied that the two genes might be involved in acrosome biogenesis, nuclear deformation, and tail formation. In mature sperm, the signals were highly condensed and co-localized in the subacrosomal space and midpiece with high intensity. In general, *kif3a/3b* mRNA is minimally or not expressed in mature sperm (Miller *et al*., 1999a; Wang *et al*., 2010; Dang *et al*., 2012; Hu *et al*., 2012). Considering that *kif3a/3b* could be detected in early embryos (Marszalek *et al*., 1999), we predict that the residual transcripts may enter eggs and thereby contribute to *P. esculenta* embryonic development.

4.2 *Pe*-KIF3A/B and Sperm Head Remodeling

MTs are highly dynamic filaments with pivotal roles in many fundamental cellular processes, including division, motility, intracellular transport, and cell shaping (Jordan and Wilson, 2004; Conde and Caceres, 2009; Helmke *et al*., 2013). During spermiogenesis, MTs are involved in sperm head remodeling, including nuclear deformation and acrosome biogenesis (Fawcett *et al*., 1971; Moreno *et al*., 2006; Zhao *et al*., 2017). In this study, MT signals could be detected in *P. esculenta* spermatids at all stages (Figs.9 and 10).

4.2.1 Nucleus reshaping

MTs are essential for sperm head remodeling (Russell *et al*., 1991; Mendoza-Lujambio *et al*., 2002; Lehti and Sironen, 2016; Dunleavy *et al*., 2017). Perinuclear MTs can interact with the nuclear envelope and karyoskeleton, thereby deforming spermatid nuclei by mechanical force (MacKinnon and Abraham, 1972; Rattner and Brinkley, 1972). As MT-dependent proteins, kinesins contribute to this process. In mice, KIF5C and KIFC1 interact with the manchette and promote nuclear deformation (Navolanic and Sperry, 2000; Kotaja *et al*., 2004; Saade *et al*., 2007). The depletion of KIF3A leads to abnormalities in the sperm head (Lehti *et al*., 2013). In addition to mammals, the functions of KIF3A/3B in nuclear deformation have been evaluated in many species, including *Larimichthys crocea*, *Larimichthys polyactis*, and *P. carinicauda* (Zhao *et al*., 2017; Mu *et al*., 2019; Wang *et al*., 2019). Our immunofluorescence analysis showed that *Pe*-KIF3A/3B co-localized with MTs throughout spermiogenesis, and their expression levels were positively correlated with the degree of nuclear deformation (Figs.9 and 10). Notably, *Pe*-KIF3A/3B signals reached a peak and were co-localized with perinuclear MTs in late-stage spermatids, along with substantial deformations, including chromatin condensation and nuclear shrinkage. Therefore, our results suggest that *Pe*-KIF3A/3B and MTs participate in the nuclear reshaping of *P. esculenta* sperm.

4.2.2 *Pe*-KIF3A/B participating in the loss of cytoplasm

Cytoplasm abandonment decreases spermatid size. In *P. esculenta*, the pseudopodia-like cytoplasmic protrusions were associated with this process. With the decline of protrusions in late spermatids, redundant cytoplasmic components and unnecessary organelles would be removed by autophagy and exocytosis. Gao *et al.* (2019) reported that MTs and KIFC1 are involved in the generation and maintenance of pseudopodia-like cytoplasmic protrusions in *P. esculenta* spermatids, indicating that cytoplasm removal relies on MTs and motor proteins.

Recent research has shown that KIF3A/3B play roles in the removal of redundant cytoplasm. As the core organelle in autophagy, lysosomes could be transported by KIF3A/3B (Brown *et al*., 2005). As a cargo of KIF3A/3B, IFT20 directs autophagy (Pampliega *et al*., 2013). Finally, Kinesin II could regulate exocytosis (Finetti *et al*., 2009). With respect to the sperm, Zhang *et al.* (2019) reported that IFT20 participates in the removal of cytoplasmic components by autophagy. Basing on the co-localization of MTs and *Pe*-KIF3A/3B observed in our study, we suggest that *Pe*-KIF3A/3B participates in cytoplasm abandonment during spermiogenesis in *P. esculenta*.

4.2.3 Acrosome biogenesis

The acrosome is an important organelle for fertilization and is formed by Golgi-secreted proacrosomal vesicles (Nolan and Hammerstedt, 1997). The proacrosomal vesicles are transported to the acroplaxome and fused to form an acrosome vesicle, finally resulting in the acrosome. During acrosome biogenesis, Kinesin II transports these vesicles along MTs (Moreno *et al*., 2006; Abraham *et al*., 2011). In *P. carinicauda*, KIF3A and tubulin are co-localized in the lamellar complex, indicating their role in acrosome formation (Zhao *et al*., 2017). In the crustacean *E. sinensis*, KIF3A and KIF3B play crucial roles in acrosome biogenesis (Yu *et al*., 2009; Lu *et al*., 2014). In mammals, Kinesin II participates in acrosome biogenesis by transporting the Golgi apparatus, endoplasmic reticulum, and lysosomes (Stauber *et al*., 2006; Brown *et al*., 2010). We observed the subcellular localization of *Pe*-KIF3A/3B and tubulin by immunofluorescence, consistent with the TEM results for the localization of proacrosomal vesicles. This observation implied that KIF3A/3B might transport the proacrosomal vesicle along MTs to form the acrosome.

4.3 *Pe*-KIF3A/3B Facilitating Sperm Tail Formation

Tails of *P. esculenta* sperm can be divided into the endpiece and the midpiece. Enflagellation is initiated in early spermatids. As is typical of ciliogenesis, enflagellation occurs in an IFT-dependent manner (Dunleavy *et al*., 2019). Several kinesins participate in sperm tail formation, including KIFC1, KIFC5, KIF17b, KLC3, and KIF3AB (Cesario and Bartles, 1994; Navolanic and Sperry, 2000; Yang and Sperry, 2003), with functions in IFT and mitochondrial transport. We focus on the roles of KIF3A/3B in tail formation in *P. esculenta*, especially in enflagellation and midpiece organization.

4.3.1 *Pe*-KIF3A/3B facilitating enflagellation

The elongation of the axoneme is the first step in enflagellation, followed by the transport of other materials along axonemal MTs to assemble the flagellum. Considering the dynamic instability of MTs, the material-trafficking cycles are needed to maintain the flagellum. Thus IFT is essential for sperm tail development and maintenance (Kozminski *et al*., 1993; Cole *et al*., 1998; Rosenbaum and Witman, 2002; Scholey, 2012). As an important anterograde motor in IFT, Kinesin II controls enflagellation (Prevo *et al*., 2017). By the transport of the IFT-B complex, kinesin-2 and KIF3A/3B are responsible for ciliary assembly (Prevo *et al*., 2017; Funabashi *et al*., 2018). Recent research on the trafficking of the IFT38–IFT52–IFT57–IFT88 complex by KIF3A/3B supports this conclusion (Funabashi *et al*., 2018). In addition, in *kif3-KO* mice, ciliary morphogenesis exhibits defects (Nonaka *et al*., 1998; Marszalek *et al*., 1999), and the depletion of KIF3A affects the elongation of the axoneme (Lehti *et al*., 2013). Moreover, IFT20, an essential subunit for enflagellation, moves in a KIF3A3/B-dependent manner (Zhang *et al*., 2019). In early spermatids, the flagellum is difficult to recognize, and the co-localized signals of KIF3A/3B and MTs are distributed evenly in the cytoplasm. With the elongation of the flagellum, the MT signals become dense in the postnuclear cytoplasm, where the flagellum forms. Axonemal MTs can also be observed. Thus, the co-localization of KIF3A/3B and MTs (especially axonemal MTs) supports the roles of *Pe*-KIF3A/3B in sperm enflagellation. Notably, *Pe*-KIF3A/3B and MTs co-localized in the flagellum of mature sperm, suggesting that *Pe*-KIF3A/3B participate in the maintenance of the flagellum. Overall, *Pe*-KIF3A/3B promote flagellum formation during spermiogenesis and facilitate the maintenance of the flagellum *via* IFT.

4.3.2 *Pe*-KIF3A/3B mediating mitochondrial behaviors during midpiece formation

The midpiece of *P. esculenta* consists of two centrioles and a helical mitochondrial sheath (Zhu *et al*., 2007). TEM showed the migration and fusion of mitochondria during spermiogenesis, which were initially evenly distributed in the cytoplasm and eventually fused into the midpiece (Fig.3). Immunofluorescence showed a similar distribution of mitochondria, and *Pe*-KIF3A/3B co-localized with mitochondria at all time points (Figs.11 and 12). These results indicate that *Pe*-KIF3A/3B participate in midpiece formation in *P. esculenta*. Some studies have suggested that KIF3A/3B are involved in mitochondrial trafficking (Zhao *et al*., 2017; Wang *et al*., 2019), and the co-localization of *Pe*-KIF3A/3B and MTs supports this hypothesis. Interestingly, heterotrimeric kinesin-2 could bind to dynactin (Mueller *et al*., 2005; Berezuk and Schroer, 2007), which can link dynein to the mitochondrial membrane surface and regulate mitochondrial transport (Deacon *et al*., 2003; Drerup *et al*., 2017). This result supports the hypothesis from

a different perspective. However, compared with Kinesin-1 and cytoplasmic dynein (Melkov and Abdu, 2017), evidence on the role of KIF3A/3B in mitochondrial transport is lacking. Notably, KIF3A/3B and dynein can bind to the same cargoes in bidirectional IFT (Andreasson *et al*., 2015). Thus, we postulated that in addition to the direct transport of mitochondria, KIF3A/3B might influence mitochondrial behaviors by mediating the functions of related proteins, such as dynein. In conclusion, we proposed that *Pe*-KIF3A/3B influence mitochondrial behaviors during midpiece formation by direct effects on transport and indirect effects on other functions.

4.4 Heterodimeric KIF3AB Participating in Spermiogenesis of *P. esculenta*

Although KIF3A/3B could act in the monomeric form, our results suggest that the heterodimeric KIF3AB has critical functions in *P. esculenta*. Compared with monomeric motors, dimeric motors have several advantages. First, in the 'step-by-step' model, two motor domains improve the coordination (Clancy *et al*., 2011; Mickolajczyk and Hancock, 2017). Second, dimeric motors are efficient transporters, especially under high-load conditions. Finally, dimers could work effectively at low concentrations (Schimert *et al*., 2019). In mammals, KIF3A and KIF3B could form heterodimeric KIF3AB in a preferential and spontaneous way (Chana *et al*., 2005). For example, the IFT-B complex could be transported by heterotrimeric kinesin-2. By contrast, other than the KIF3AB heterodimer, the monomeric KIF3A/3B and dimers of KIF3A/3B could not complete these normal functions. Our immunofluorescence analysis showed that *Pe*-KIF3A co-localized with *Pe*-KIF3B at all stages of spermiogenesis, indicating the direct interaction between the two proteins. These findings suggest that *Pe*-KIF3A/3B participate in spermiogenesis of *P. esculenta* in the form of *Pe*-KIF3AB.

5 Conclusions

This is the first study of KIF3A/3B proteins in *P. esculenta*. We provide a detailed description of spermiogenesis in the species through HE staining and TEM. We detected the mRNA expression patterns of *Pe-kif3a/3b*, which are ubiquitously expressed with particularly high levels in sperm masses. Immunofluorescence showed the consistent co-localization of MTs and *Pe*-KIF3A/3B, indicating their potential functions in sperm head remodeling and tail formation. The co-localization of *Pe*-KIF3A/3B and mitochondria suggests that they function in midpiece formation because the functions of KIF3A/3B are conservative. Therefore, a creditable model of protein functions was proposed (Fig.14b). In addition, our findings suggest that heterodimeric *Pe*-KIF3AB participates in sperm head remodeling, including nuclear reshaping, cytoplasm abandonment, and acrosome biogenesis. *Pe*-KIF3AB also has potential functions in sperm tail formation by facilitating sperm enflagellation and mediating mitochondrial behavior during midpiece formation.

Acknowledgements

The authors are grateful to all members of the Fish Histology Laboratory in Ningbo University for providing direct assistance and constructive discussions for this research. This project was supported by the Ningbo Science and Technology Plan Projects (Nos. 2019B10016, 2016C 10004), the Major Science and Technology Projects in Zhejiang Province (No. 2011C12013), the Natural Science Foundation of Zhejiang Province (No. LY18C190007), the National Natural Science Foundation of China (No. 312 72642), the Collaborative Innovation Center for Marine High-efficiency and Healthy Aquaculture of Zhejiang Province, and K. C. Wong Magna Fund in Ningbo University.

References

Amaral, A., Lourenço, B., Marques, M., and Ramalhosantos, J., 2013. Mitochondria functionality and sperm quality. *Reproduction*, **146** (5): 163-174.

Andreasson, J. O., Shastry, S., Hancock, W. O., and Block, S. M., 2015. The mechanochemical cycle of mammalian kinesin-2 KIF3A/B under load. *Current Biology*, **25** (9): 1166-1175.

Berezuk, M. A., and Schroer, T. A., 2007. Dynactin enhances the processivity of kinesin-2. *Traffic*, **8** (2): 124-129.

Brown, C. L., Maier, K. C., Stauber, T., Ginkel, L. M., Wordeman, L., Vernos, I., *et al*., 2005. Kinesin-2 is a motor for late endosomes and lysosomes. *Traffic*, **6** (12): 1114-1124.

Cesario, M. M., and Bartles, J. R., 1994. Compartmentalization, processing and redistribution of the plasma membrane protein CE9 on rodent spermatozoa. *Journal of Cell Science*, **107** (4): 561-570.

Chana, M. S., Tripet, B. P., Mant, C. T., and Hodges, R., 2005. Stability and specificity of heterodimer formation for the coiled-coil neck regions of the motor proteins KIF3A and KIF3B: The role of unstructured oppositely charged regions. *Journal of Peptide Research*, **65** (2): 209-220.

Clancy, B. E., Behnke-Parks, W. M., Andreasson, J. O., Rosenfeld, S. S., and Block, S. M., 2011. A universal pathway for kinesin stepping. *Nature Structural & Molecular Biology*, **18** (9): 1020-1027.

Cole, D. G., Diener, D. R., Himelblau, A. L., Beech, P. L., Fuster, J. C., and Rosenbaum, J. L., 1998. Chlamydomonas kinesin-II-dependent intraflagellar transport (IFT): IFT particles contain proteins required for ciliary assembly in *Caenorhabditis elegans* sensory neurons. *Journal of Cell Biology*, **141** (4): 993-1008.

Conde, C., and Caceres, A., 2009. Microtubule assembly, organization and dynamics in axons and dendrites. *Nature Reviews Neuroscience*, **10** (5): 319-332.

Dang, R., Zhu, J. Q., Tan, F. Q., Wang, W., Zhou, H., and Yang, W. X., 2012. Molecular characterization of a KIF3B-like kinesin gene in the testis of *Octopus tankahkeei* (Cephalopoda, Octopus). *Molecular Biology Reports*, **39** (5): 5589-5598.

Deacon, S. W., Serpinskaya, A. S., Vaughan, P. S., Lopez-Fanarraga, M., Vernos, I., Vaughan, K. T., *et al*., 2003. Dynactin is required for bidirectional organelle transport. *Journal of Cell Biology*, **160** (3): 297-301.

DeCuevas, M., Tao, T., and Goldstein, L. S. B., 1992. Evidence that the stalk of *Drosophila* kinesin heavy chain is an a-helical coiled coil. *The Journal of Cell Biology*, **116**: 957-965.

Drerup, C. M., Herbert, A. L., Monk, K. R., and Nechiporuk, A. V., 2017. Regulation of mitochondria-dynactin interaction and

mitochondrial retrograde transport in axons. *eLife*, **6**: e22234.
Dunleavy, J. E. M., O'Bryan, M. K., Stanton, P. G., and O'Donnell, L., 2019. The cytoskeleton in spermatogenesis. *Reproduction*, **157** (2): 53-72.
Dunleavy, J. E., Okuda, H., O'connor, A. E., Merriner, D. J., O'Donnell, L., Jamsai, D., *et al*., 2017. Katanin-like 2 (KATNAL2) functions in multiple aspects of haploid male germ cell development in the mouse. *PLoS Genetics*, **13** (11): e1007078.
Fan, J., and Beck, K. A., 2004. A role for the spectrin superfamily member Syne-1 and kinesin II in cytokinesis. *Journal of Cell Science*, **117** (4): 619-629.
Fawcett, D. W., Anderson, W. A., and Phillips, D. M., 1971. Morphogenetic factors influencing the shape of the sperm head. *Developmental Biology*, **26** (2): 220-251.
Finetti, F., Paccani, S. R., Riparbelli, M. G., Giacomello, E., Perinetti, G., Pazour, G. J., *et al*., 2009. Intraflagellar transport is required for polarized recycling of the TCR/CD3 complex to the immune synapse. *Nature Cell Biology*, **11** (11): 1332-1339.
Funabashi, T., Katoh, Y., Okazaki, M., Sugawa, M., and Nakayama, K., 2018. Interaction of heterotrimeric kinesin-II with IFT-B-connecting tetramer is crucial for ciliogenesis. *Journal of Cell Biology*, **217** (8): 2867-2876.
Gao, X. M., Mu, D. L., Hou, C. C., Zhu, J. Q., Jin, S., and Wang, C. L., 2019. Expression and putative functions of KIFC1 for nuclear reshaping and midpiece formation during spermiogenesis of *Phascolosoma esculenta*. *Gene*, **683**: 169-183.
Gilbert, S. P., Guzik-Lendrum, S., and Rayment, I., 2018. Kinesin-2 motors: Kinetics and biophysics. *The Journal of Biological Chemistry*, **293** (12): 4510-4518.
Guzik-Lendrum, S., Rank, K. C., Bensel, B. M., Taylor, K. C., Rayment, I., and Gilbert, S. P., 2015. Kinesin-2 KIF3AC and KIF3AB can drive long-range transport along microtubules. *Biophysical Journal*, **109** (7): 1472-1482.
Hall, E. S., Eveleth, J., Jiang, C., Redenbach, D. M., and Boekelheide, K., 1992. Distribution of the microtubule-dependent motors cytoplasmic dynein and kinesin in rat testis. *Biology of Reproduction*, **46** (5): 817-828.
Haraguchi, K., Hayashi, T., Jimbo, T., Yamamoto, T., and Akiyama, T., 2006. Role of the kinesin-2 family protein, KIF3, during mitosis. *Journal of Biological Chemistry*, **281** (7): 4094-4099.
Helmke, K. J., Heald, R., and Wilbur, J. D., 2013. Interplay between spindle architecture and function. *International Review of Cell and Molecular Biology*, **306**: 83-125.
Henson, J. H., Cole, D. G., Roesener, C. D., Capuano, S., Mendola, R. J., and Scholey, J. M., 1997. The heterotrimeric motor protein kinesin-II localizes to the midpiece and flagellum of sea urchin and sand dollar sperm. *Cell Motility & the Cytoskeleton*, **38** (1): 29-37.
Hirokawa, N., and Noda, Y., 2008. Intracellular transport and kinesin superfamily proteins, KIFs: Structure, function, and dynamics. *Physiological Reviews*, **88** (3): 1089-1118.
Hu, J. R., Xu, N., Tan, F. Q., Wang, D. H., Liu, M., and Yang, W. X., 2012. Molecular characterization of a KIF3A-like kinesin gene in the testis of the Chinese fire-bellied newt *Cynops orientalis*. *Molecular Biology Reports*, **39** (4): 4207-4214.
Jordan, M. A., and Wilson, L., 2004. Microtubules as a target for anticancer drugs. *Nature Reviews Cancer*, **4** (4): 253-265.
Kierszenbaum, A. L., Rivkin, E., and Tres, L. L., 2011. Cytoskeletal track selection during cargo transport in spermatids is relevant to male fertility. *Spermatogenesis*, **1** (3): 221-230.
Kodani, A., Salomé, S. M., Seol, A., Garciaverdugo, J. M., and Reiter, J. F., 2013. Kif3a interacts with Dynactin subunit $p150^{Glued}$ to organize centriole subdistal appendages. *Embo Journal*, **32** (4): 597-607.
Kotaja, N., De-Cesare, D., Macho, B., Monaco, L., Brancorsini, S., Goossens, E., *et al*., 2004. Abnormal sperm in mice with targeted deletion of the act (activator of cAMP-responsive element modulator in testis) gene. *PNAS*, **101** (29): 10620-10625.
Kozminski, K. G., Johnson, K. A., Forscher, P., and Rosenbaum, J. L., 1993. A motility in the eukaryotic flagellum unrelated to flagellar beating. *PNAS*, **90** (12): 5519-5523.
Lehti, M. S., and Sironen, A., 2016. Formation and function of the manchette and flagellum during spermatogenesis. *Reproduction*, **151** (4): R43-R54.
Lehti, M. S., Kotaja, N., and Sironen, A., 2013. KIF3A is essential for sperm tail formation and manchette function. *Molecular & Cellular Endocrinology*, **377** (1-2): 44-55.
Li, F. L., 1992. A checklist of sipuncula from the China coasts. *Journal of Ocean University of Qingdao*, **22** (2): 72-88.
Long, L. L., Sheng, Z., and Zhu, J. Q., 2015. Ultrastructural observations on spermiogenesis in the peanut worm, *Phascolosoma esculenta* (Sipuncula: *Phascolosomatidea*). *Animal Cells & Systems*, **19** (3): 1-9.
Lu, Y., Wang, Q., Wang, D. H., Zhou, H., Hu, Y. J., and Yang, W. X., 2014. Functional analysis of KIF3A and KIF3B during spermiogenesis of Chinese mitten crab *Eriocheir sinensis*. *PLoS One*, **9** (5): e97645.
Ma, D. D., Wang, D. H., and Yang, W. X., 2017. Kinesins in spermatogenesis. *Biology of Reproduction*, **96** (2): 267-276.
MacKinnon, E. A., and Abraham, J. P., 1972. The manchette in stage 14 rat spermatids: A possible structural relationship with the redundant nuclear envelope. *Zeitschrift für Zellforschung und Mikroskopische Anatomie*, **124** (1): 1-11.
Marszalek, J. R., and Goldstein, L. S., 2000. Understanding the functions of kinesin-II. *Biochimica et Biophysica Acta*, **1496** (1): 142-150.
Marszalek, J. R., Liu, X., Roberts, E. A., Chui, D., Marth, J. D., Williams, D. S., *et al*., 2000. Genetic evidence for selective transport of opsin and arrestin by kinesin-II in mammalian photoreceptors. *Cell*, **102** (2): 175-187.
Marszalek, J. R., Ruiz-Lozano, P., Roberts, E., Chien, K. R., and Goldstein, L. S., 1999. Situs inversus and embryonic ciliary morphogenesis defects in mouse mutants lacking the KIF3A subunit of kinesin-II. *PNAS*, **96** (9): 5043-5048.
Melkov, A., and Abdu, U., 2017. Regulation of long-distance transport of mitochondria along microtubules. *Cellular and Molecular Life Sciences*, **75** (2): 163-176.
Mendoza-Lujambio, I., Burfeind, P., Dixkens, C., Meinhardt, A., Hoyer-Fender, S., Engel, W., *et al*., 2002. The Hook1 gene is non-functional in the abnormal spermatozoon head shape (azh) mutant mouse. *Human Molecular Genetics*, **11** (14): 1647-1658.
Mickolajczyk, K. J., and Hancock, W. O., 2017. Kinesin processivity is determined by a kinetic race from a vulnerable one-head-bound state. *Biophysical Journal*, **112** (12): 2615-2623.
Miki, H., Okada, Y., and Hirokawa, N., 2005. Analysis of the kinesin superfamily: Insights into structure and function. *Trends in Cell Biology*, **15** (9): 467-476.
Miller, D., Briggs, D., Snowden, H., Hamlington, J., Rollinson, S., Lilford, R., *et al*., 1999a. A complex population of RNAs exists in human ejaculate spermatozoa: Implications for understanding molecular aspects of spermiogenesis. *Gene*, **237** (2): 385-392.
Miller, M. G., Mulholl, D. J., and Vogl, A. W., 1999b. Rat testis motor proteins associated with spermatid translocation (dynein) and spermatid flagella (kinesin-II). *Biology of Reproduction*, **60** (4): 1047-1056.
Moreno, R. D., Palomino, J., and Schatten, G., 2006. Assembly of spermatid acrosome depends on microtubule organization during mammalian spermiogenesis. *Developmental Biology*, **293**

(1): 218-227.

Mu, D. L., Du, C., Fu, S. Y., Wang, J. Q., Hou, C. C., Tang, D. J., *et al*., 2019. Molecular characterization, tissue distribution and localization of *Larimichthys crocea* Kif3a and Kif3b and expression analysis of their genes during spermiogenesis. *Journal of Ocean University of China*, **18** (6): 1451-1469.

Mueller, J., Perrone, C. A., Bower, R., Cole, D. G., and Porter, M. E., 2005. The FLA3 KAP subunit is required for localization of kinesin-2 to the site of flagellar assembly and processive anterograde intraflagellar transport. *Molecular Biology of the Cell*, **16** (3): 1341-1354.

Navolanic, P. M., and Sperry, A. O., 2000. Identification of isoforms of a mitotic motor in mammalian spermatogenesis. *Biology of Reproduction*, **62** (5): 1360-1369.

Nolan, J. P., and Hammerstedt, R. H., 1997. Regulation of membrane stability and the acrosome reaction in mammalian sperm. *The FASEB Journal*, **11** (8): 670-682.

Nonaka, S., Tanaka, Y., Okada, Y., Takeda, S., Harada, A., Kanai, Y., *et al*., 1998. Randomization of left-right asymmetry due to loss of nodal cilia generating leftward flow of extraembryonic fluid in mice lacking KIF3B motor protein. *Cell*, **95** (6): 829-837.

Nuurai, P., Panasophonkul, S., Tinikul, Y., Sobhon, P., and Wanichanon, R., 2016. Spermatogenesis in the rock oyster, *Saccostrea forskali* (Gmelin, 1791). *Tissue & Cell*, **48** (1): 43-48.

O'Donnell, L., and O'Bryan, M. K., 2014. Microtubules and spermatogenesis. *Seminars in Cell & Developmental Biology*, **30**: 45-54.

Pampliega, O., Orhon, I., Patel, B., Sridhar, S., Diaz-Carretero, A., Beau, I., *et al*., 2013. Functional interaction between autophagy and ciliogenesis. *Nature*, **502** (7470): 194-200.

Pan, X., Ou, G., Civelekogluscholey, G., Blacque, O. E., Endres, N. F., Tao, L., *et al*., 2006. Mechanism of transport of IFT particles in *C. elegans* cilia by the concerted action of kinesin-II and OSM-3 motors. *Journal of Cell Biology*, **174** (7): 1035-1045.

Prevo, B., Scholey, J. M., and Peterman, E. J. G., 2017. Intraflagellar transport: Mechanisms of motor action, cooperation, and cargo delivery. *FEBS Journal*, **284** (18): 2905-2931.

Ramalhosantos, J., Varum, S., Amaral, S., Mota, P. C., Sousa, A. P., and Amaral, A., 2009. Mitochondrial functionality in reproduction: From gonads and gametes to embryos and embryonic stem cells. *Human Reproduction Update*, **15** (5): 553-572.

Rashid, D. J., Wedaman, K, P., and Scholey, J. M., 1995. Heterodimerization of the two motor subunits of the heterotrimeric kinesin, KRP(85/95). *Journal of Molecular Biology*, **252** (2): 157-162.

Rattner, J. B., and Brinkley, B. R., 1972. Ultrastructure of mammalian spermiogenesis. 3. The organization and morphogenesis of the manchette during rodent spermiogenesis. *Journal of Ultrastructure Research*, **41** (3): 209-218.

Rosenbaum, J. L., and Witman, G. B., 2002. Intraflagellar transport. *Nature Reviews Molecular Cell Biology*, **3** (11): 813-825.

Rupik, W., Huszno, J., and Klag, J., 2011. Cellular organisation of the mature testes and stages of spermiogenesis in *Danio rerio* (Cyprinidae; Teleostei)–structural and ultrastructural studies. *Micron*, **42** (8): 833.

Russell, L. D., Russell, J. A., MacGregor, G. R., and Meistrich, M. L., 1991. Linkage of manchette microtubules to the nuclear envelope and observations of therole of the manchette in nuclear shaping during spermiogenesis in rodents. *American Journal of Anatomy*, **192** (2): 97-120.

Saade, M., Irla, M., Govin, J., Victorero, G., Samson, M., and Nguyen, C., 2007. Dynamic distribution of spatial during mouse spermatogenesis and its interaction with the kinesin KIF17b. *Experimental Cell Research*, **313** (3): 614-626.

Schimert, K. I., Budaitis, B. G., Reinemann, D. N., Lang, M. J., and Verhey, K. J., 2019. Intracellular cargo transport by single-headed kinesin motors. *PNAS*, **116** (13): 6152-6161.

Scholey, J. M., 2012. Kinesin-2 motors transport IFT-particles, dyneins and tubulin subunits to the tips of *Caenorhabditis elegans* sensory cilia: Relevance to vision research? *Vesion Research*, **75**: 44-52.

Shen, H. Q., Xiao, Y. X., She, Z. Y., Tan, F. Q., and Yang, W. X., 2017. A novel role of KIF3b in the seminoma cell cycle. *Experimental Cell Research*, **352** (1): 95-103.

Singson, A., 2001. Every sperm is sacred: Fertilization in *Caenorhabditis elegans*. *Developmental Biology*, **230** (2): 101-109.

Stauber, T., Simpson, J. C., and Pepperkok, R., 2006. A role for kinesin-2 in COPI-dependent recycling between the ER and the golgi complex. *Current Biology*, **16** (22): 2245-2251.

Su, X. R., Du, L. L., Li, Y. Y., Li, Y., Zhou, J., and Li, T., 2010. Cloning and expression of HSP70 gene ofsipuncula *Phascolosoma esculenta. Fish and Shellfish Immunology*, **28** (3): 461-466.

Wang, J. Q., Gao, X. M., Zheng, X. B., Hou, C. C., Xie, Q. P., Lou, B., *et al*., 2019. Expression and potential functions of KIF3A/3B to promote nuclear reshaping and tail formation during *Larimichthys polyactis* spermiogenesis. *Development Genes and Evolution*, **229** (5-6): 161-181.

Wang, W., Dang, R., Zhu, J. Q., and Yang, W. X., 2010. Identification and dynamic transcription of KIF3A homologue gene in spermiogenesis of *Octopus tankahkeei*. *Comparative Biochemistry & Physiology Part A Molecular & Integrative Physiology*, **157** (3): 237-245.

Yamazaki, H., Nakata, T., Okada, Y., and Hirokawa, N., 1994. KIF3B forms a heterodimer with KIF3A and works as a new microtubule-based anterograde motor of membrane organelle transport. *Neuroscience Research Supplements*, **19**: S84.

Yamazaki, H., Nakata, T., Okada, Y., and Hirokawa, N., 1996. Cloning and characterization of KAP3: A novel kinesin superfamily-associated protein of KIF3A/3B. *PNAS*, **93** (16): 8443-8448.

Yang, W. X., and Sperry, A. O., 2003. C-terminal kinesin motor KIFC1 participates in acrosome biogenesis and vesicle transport. *Biology Reproduction*, **69** (5): 1719-1729.

Yang, Z., Roberts, E. A., and Goldstein, L. S., 2001. Functional analysis of mouse kinesin motor Kif3C. *Molecular and Cellular Biology*, **21** (16): 5306-5311.

Yu, K., Hou, L., Zhu, J. Q., Ying, X. P., and Yang, W. X., 2009. KIFC1 participates in acrosomal biogenesis, with discussion of its importance for the perforatorium in the Chinese mitten crab *Eriocheir sinensis*. *Cell & Tissue Research*, **337** (1): 113-123.

Zhang, Z. G., Li, W., Zhang, Y., Zhang, L., Teves, M., Liu, H., *et al*., 2016. Intraflagellar transport protein IFT20 is essential for male fertility and spermiogenesis in mice. *Journal of Molecular Cell Biology*, **27** (23): 3705-3716.

Zhao, Y. Q., Mu, D. L., Wang, D., Han, Y. L., Hou, C. C., and Zhu, J. Q., 2018. Analysis of the function of KIF3A and KIF3B in the spermatogenesis in *Boleophthalmus pectinirostris*. *Fish Physiology and Biochemistry*, **44** (3): 769-788.

Zhao, Y. Q., Yang, H. Y., Zhang, D. D., Han, Y. L., Hou, C. C., and Zhu, J. Q., 2017. Dynamic transcription and expression patterns of KIF3A and KIF3B genes during spermiogenesis in the shrimp, *Palaemon carincauda*. *Animal Reproduction Science*, **184**: 59-77.

Zhu, J. Q., Wang, W., Xu, S. J., and Zeng, H. X., 2007. Spermatogenesis and sperm morphology of *Phascolosoma esculenta*. *Acta Zoologica Sinica*, **53** (4): 733-741.

(Edited by Qiu Yantao)